1-1-1999

Finite element simulation of chip formation in orthogonal metal cutting using the Langrangian formulation in DYNA3D

Benjamen David McClain
Iowa State University

Finite element simulation of chip formation in orthogonal metal cutting using the Langrangian formulation in DYNA3D

by

Benjamen David McClain

A thesis submitted to the graduate faculty

in partial fulfillment of the requirements for the degree of

MASTER OF SCIENCE

Major: Mechanical Engineering

Major Professors: G. Ivan Maldonado and Stephen A. Batzer

Iowa State University

Ames, Iowa

1999

Graduate College
Iowa State University

This is to certify that the Master's thesis of

Benjamen David McClain

has met the thesis requirements of Iowa State University

Signatures have been redacted for privacy

TABLE OF CONTENTS

LIST OF TABLES

LIST OF FIGURES

1 OVERVIEW

1.1 Introduction

Machining is one of the most common manufacturing processes. Machining can include such material removal processes as abrasion, cutting, or non-traditional processes like electrical, chemical, or optical removal of material. Metal cutting accounts for a large percentage of machining operations. In metal cutting, unwanted material is removed in the form of chips. This includes such processes as turning, milling, drilling, and boring. Consequently, studying the process of chip formation can give important insights into many typical machining operations.

Many machining studies have been performed over the years, but the chip formation process is still not completely understood. This is due in part to the high speed nature of machining, the small size of the chips which are formed, and the complex nature of the phenomena involved. It is necessary to consider such factors as friction, strain rate, thermal effects, and the mechanical properties of the workpiece and tool material to completely characterize the chip formation process. As it is difficult to gain a complete understanding of the chip formation process through machining experiments, numerical methods such as finite element modeling (FEM) can be useful. With an FEM simulation, it is possible to carefully analyze the process by manipulating the control parameters involved and take a closer look at the state of the chip, thereby increasing the understanding of metal cutting.

1.2 Thesis Organization

This thesis is laid out in four chapters. The first chapter gives an introduction to the mechanics of metal cutting, as well as the principles of finite element modeling. The research approach for this thesis is described, and the relevant literature in the field of metal cutting simulation is reviewed. The second chapter contains a paper which has been submitted to the Journal of Machining Science and Technology. In this paper, FEM is used to compare the effects of varying geometries of grooved cutting tools. The third chapter contains a paper detailing improvements on the previous simulations and provides vali-

dation of the FEM machining model through comparisons with experimental machining observations. Finally, the fourth chapter presents a discussion of the research results and gives recommendations for future work.

1.3 Principles of Metal Cutting

In metal cutting, a tool is used to scrape away unwanted material, which forms chips. Metal cutting includes varied processes such as milling, drilling, turning, and boring. Although the processes are different, they each produce chips in a similar fashion. Therefore, analysis of chip formation can shed light on the mechanics of each machining process. Cutting processes may be characterized as orthogonal or oblique as shown in Figure 1.1. In orthogonal cutting, the cutting edge of the tool is perpendicular to the tool's motion and the motion of the chip occurs in a plane. The properties of the chip are considered to be uniform across its width. As a result, orthogonal cutting may be characterized by studying a cross-section of the chip. In oblique cutting, the cutting edge of the tool is inclined at an angle, and the chip is directed to the side. This thesis is primarily devoted to the study and modeling of orthogonal cutting, nevertheless, some leads and insights have been provided for the subject of oblique cutting, which logically follows as an area for future research.

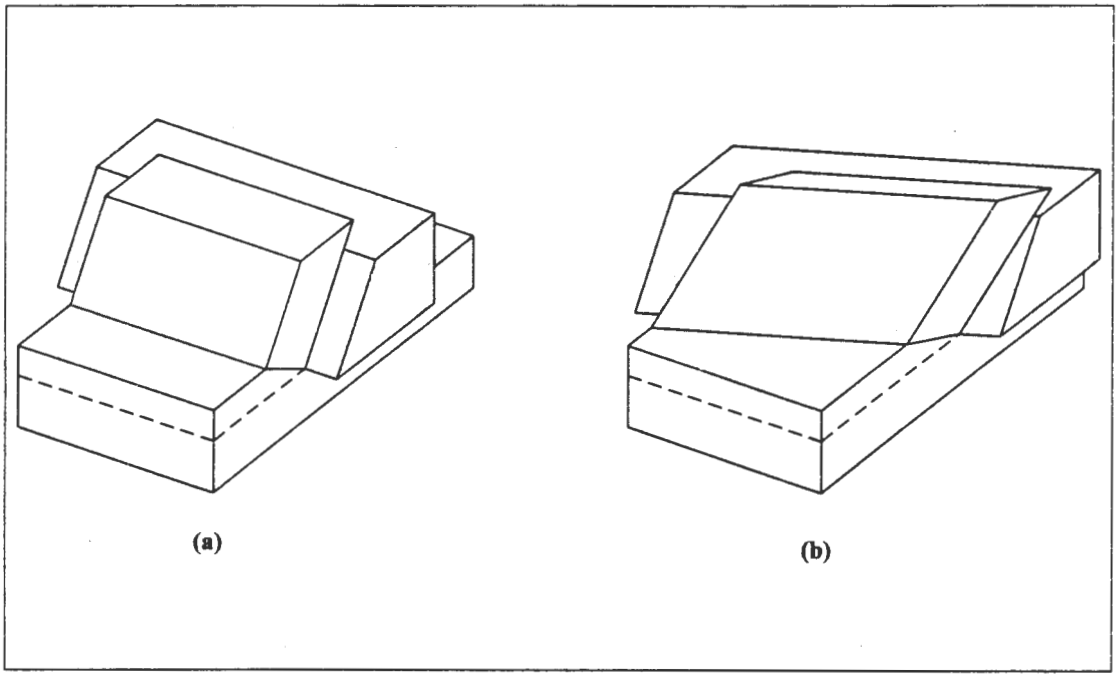

Figure 1.1 (a) orthogonal cutting (b) oblique cutting

The basic terms describing the orthogonal cutting process are illustrated in Figure 1.2. In this figure, the tool is fixed and the workpiece moves toward it at a prescribed velocity. This velocity is known as the cutting speed. The depth of the cut, t_o, is known as the undeformed chip thickness. Note that the thickness of the chip, t_c, is greater than the undeformed chip thickness. These thicknesses are related by the shear plane angle, ϕ. The shear plane angle is an important characteristic in metal cutting that varies with varying cutting conditions and workpiece materials. Much work has gone into deriving a model that can accurately predict ϕ for a given cutting situation [1-4].

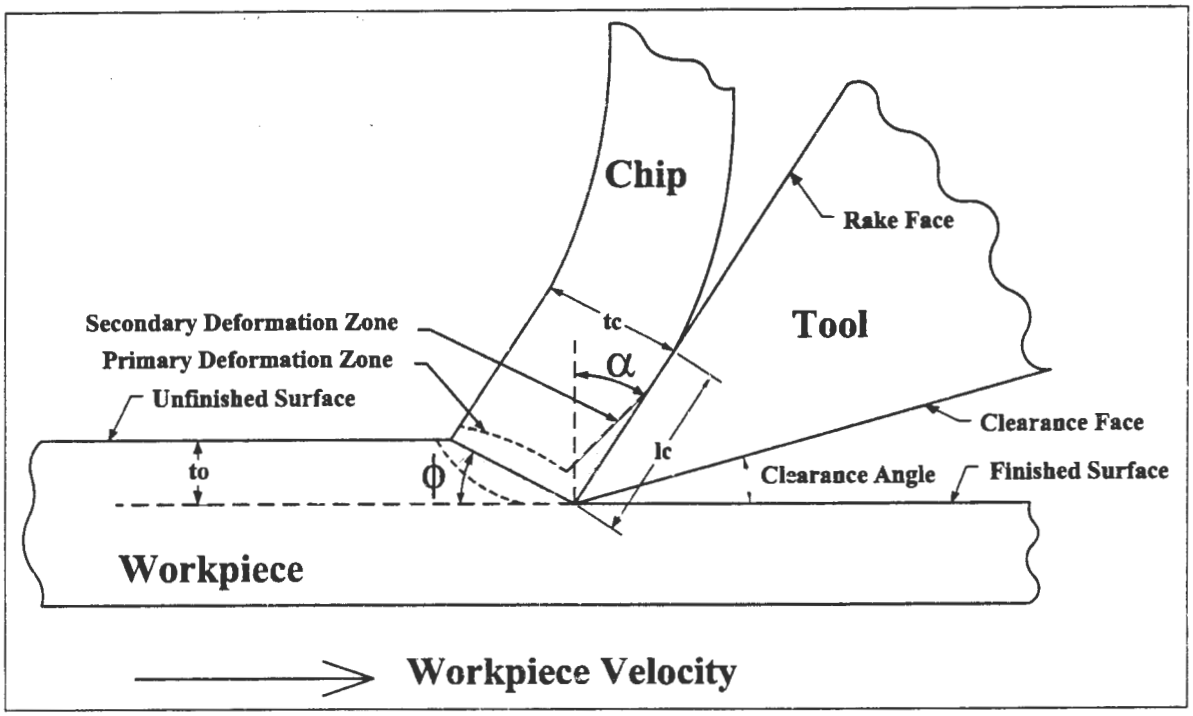

Figure 1.2 Orthogonal cutting terminology

The face of the tool that comes in contact with the chip is known as the rake face, and the trailing edge of the tool is known as the clearance face. The angle between the rake face and the normal to the workpiece surface is known as the rake angle, α. Different rake angles are used for different cutting situations. When the rake face of the tool is located in the clockwise direction from the workpiece normal, as shown in Figure 1.2, the rake angle is considered to be positive. The rake angle is considered to be negative when the rake face of the tool is located in the counterclockwise direction from the workpiece normal. A small clearance angle is generally included in the tool to keep the clearance face from spoiling the finished surface.

Chips are formed by plastic deformation, and two deformation zones may be observed [5]. The

primary deformation zone stretches from the tool tip to the free surface of the workpiece, and the secondary deformation zone exists in the region where the chip is in contact with the cutting tool. The primary deformation zone is a narrow region where the chip experiences large strains. In the secondary deformation zone, the chip is affected by the friction between the chip and the tool.

The length of contact between the chip and tool, l_c, can have a significant impact on the cutting forces. As a result, some tools are designed with grooves to reduce l_c. These tools are known as restricted contact tools. These grooves can also help cause the chip to break. Machining of ductile materials can result in the production of long continuous chips. These chips may become entangled in the machine, causing delays in production and danger for the operator. Therefore, it is desirable to have a method to break the chips. This is often accomplished by using chip breakers in the form of grooved tools or flat faced tools with obstructions added as shown in Figure 1.3.

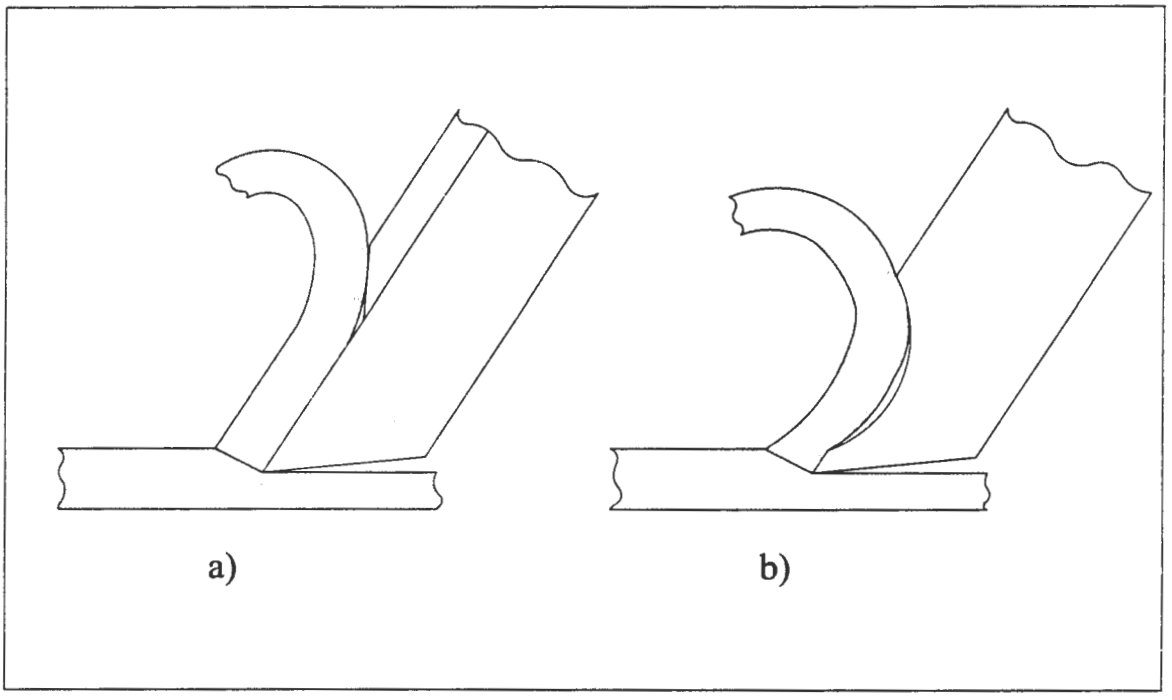

Figure 1.3 (a) obstruction chip breaker (b) grooved chip breaker

Large forces may be generated in metal cutting due to the high speed nature of machining. The forces in orthogonal cutting are shown in Figure 1.4. The cutting force, F_c, acts in the direction of the cutting speed V. The thrust force, F_t, acts in the direction perpendicular to the workpiece, normal to the cutting velocity. The cutting force is generally the larger of the two forces and supplies most of the energy for machining.

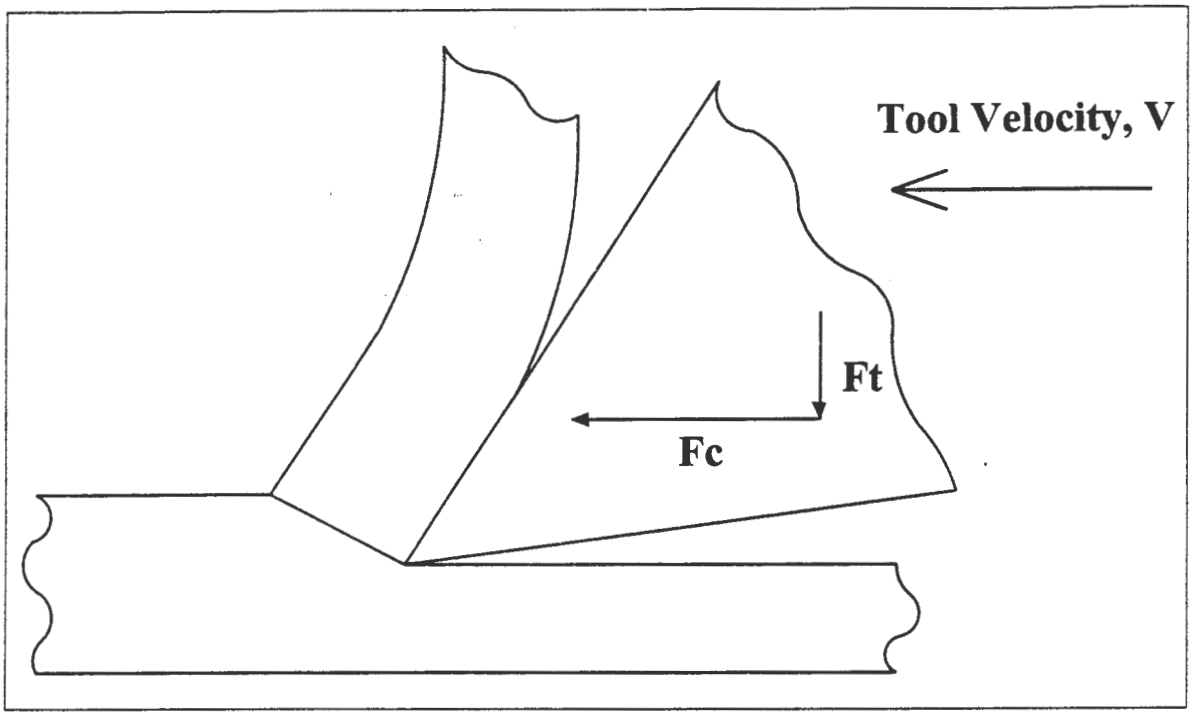

Figure 1.4 Forces in orthogonal cutting

1.4 Principles of Finite Element Modeling

Finite element analysis is a numerical method used to calculate approximate solutions to problems which would typically be expressed in terms of differential equations [6]. In the finite element method, complex objects are partitioned into small simply shaped regions called elements. These elements typically have a brick or triangular shape. The solution to the problem is determined by numerically solving for the variable of interest at specified points, called nodes, on each individual element and then applying those solutions to the object as a whole. The differential equations describing the behavior of the structure are simplified to a set of algebraic equations in order to be solved numerically. As a result, the solution of a finite element analysis is generally not an exact solution. Although not an exact solution, the finite element method may be used to produce close approximations to the exact solutions for problems that would be difficult, or impossible, to solve exactly. Developments in finite element theory coupled with advances in computer technology have caused the finite element method to rapidly increase in popularity over the last 20 years.

The first step in a finite element analysis is to discretize the structure [7]. In this step, the structure is divided into small regions, or finite elements. Next, the properties of the elements are defined. Different types of elements may be used depending on the requirements of the analysis. A stiffness matrix

is defined which determines the behavior of the element under loading. Next, loads such as forces, moments, and velocities are applied. Boundary conditions are then defined. The boundary conditions define the displacements of specified nodes. Finally, the element descriptions, loads, and boundary conditions are assembled as a set of linear equations in matrix form. This set of equations will be solved numerically for the unknown values, the nodal displacements. In what is known as the post-processing stage, the nodal displacements are used to calculate properties of interest, like the stresses or strains in the structure.

In general the equilibrium equations for a finite element analysis may be expressed in the following form:

$$\{F\} = [K]\{U\} \tag{1.1}$$

where F is the vector matrix giving the forces on the element, K is the element stiffness matrix, and U is the vector matrix of nodal displacements to be determined. The sizes of these matrices will vary with the number of elements used to make up the structure and the number of nodes per element. Equation 1.1 is a simplified form of the equations used in a finite element model. These equations become more complicated when considering factors such as nonlinear material properties and friction.

Two different viewpoints may be used to describe a continuous medium with a finite element model [2]. The first viewpoint focuses on a fixed point in space and considers all matter that passes through that point. This viewpoint, known as the Eulerian formulation, is concerned with changes in the matter that passes through one particular point. The changes could involve such characteristics as velocity, pressure, or density. The Eulerian formulation is typically used to describe the motion of fluids, but it has been applied to metal cutting problems because it only requires a small number of elements. Therefore, it is computationally efficient. The Eulerian formulation is also advantageous in metal cutting problems because it is unnecessary to predefine the line where the chip separates from the workpiece. However, due to the nature of the Eulerian formulation, it is only possible to simulate steady-state cutting. The incipient stages of chip formation cannot be simulated.

The second viewpoint used to describe a continuous medium is the Lagrangian formulation. This description is used in the study of solid bodies, including most metal cutting simulations. The Lagrangian formulation focuses on a fixed set of material particles and follows them regardless of their location. The Lagrangian formulation may be used to completely predict the final deformed shape of an object, whereas with the Eulerian formulation assumptions must be made about the object's final shape. As a result, the Lagrangian formulation may be used to completely simulate the formation of a chip, from the

incipient stages to steady-state cutting. This has made the Lagrangian description the most popular method for metal cutting simulations, despite a number of disadvantages. The Lagrangian description requires the use of a larger number of elements, and is therefore more computationally intensive. In addition, it is necessary to predefine the line where the chip will separate from the workpiece and establish a criterion to determine when the elements will separate.

1.5 Literature Review

The machining process is quite complex due to the high speeds, strain rates, and thermal effects involved. Although researchers have been trying to develop metal cutting models for years, the process is still not completely understood. The first machining models were analytical in nature and were based mainly on experimental observations, but numerical methods have gained increasing popularity since the 1970's.

1.5.1 Analytical Models

Some of the early attempts to develop an analytical machining model focused on predicting the shear plane angle, ϕ. In 1941, Ernst and Merchant used a minimum energy approach and proposed an equation that predicted ϕ based on the rake angle of the tool and the coefficient of friction between the tool and workpiece [1]. A more sophisticated model was developed in 1951 by Lee and Schaffer [2], but neither model successfully predicted ϕ for all workpiece materials and cutting conditions. In 1966, Rowe and Spick reevaluated the minimum energy approach without specifying the coefficient of friction between the chip and tool in an attempt to develop a model applicable to a wider range of materials and conditions [3]. A more advanced model was developed in by Wright in 1982 [4]. This model predicted the shear plane angle based on the rake angle and the shear and ultimate strengths of the workpiece material, but it did not account for friction or thermal effects encountered in high speed cutting.

Other researchers have focused their attention on the modeling of chip curl and chip breaking mechanisms. Much work in this field has been done by Nakayama [9, 10]. Nakayama analyzed the curl of the chips in metal cutting and performed extensive studies on chip breaking mechanisms, developing an analytical criterion for chip breaking. In 1990, Jawahir used high speed filming to study chip flow mechanisms and develop an approximate cutting force model [11]. In a later study, Jawahir developed an analytical model for the bending moments along the length of a curled chip when using flat faced cutting tools [12]. In addition, the backwall forces in grooved tool cutting were modeled. In a 1996 work by Fang and Jawahir [13], an analytical chip breaking model was developed which predicted the

forces and bending moments on the chip, the chip thickness and velocity, the tool-chip contact length, and the shear and friction angles.

1.5.2 Numerical Models

Although there has been much work done in the field, analytical modeling of chip formation has proven to be exceedingly complex. As a result, numerical methods, finite element modeling in particular, have become increasingly popular. Finite element models have been developed by many researchers since the 1970's. The vast majority of these models have focused on orthogonal metal cutting, although some limited models of oblique cutting have been developed [14, 15]. Some of the models have used the Eulerian formulation, but most have relied on a Lagrangian formulation which allows the chip to be modeled from incipient to steady-state cutting.

One of the first finite element models of machining was developed by Klamecki in 1973 [16]. This was a three-dimensional model of incipient chip formation in metal cutting. Another early model was developed in 1974 by Tay [17]. This was a two-dimensional model used to calculate temperature distributions in steady-state orthogonal cutting. A drawback of this model was that it required the input of experimental strain rate data.

In the last two decades, improved models have been developed by many researchers. Strenkowski has done significant work in the field. In 1985, Strenkowski and Carroll developed a finite element model based on the Lagrangian formulation that modeled chip formation from incipient to steady-state cutting [18]. This model included the effects of friction and heat generation, as well as a separation criterion based on effective plastic strain. A later model by Strenkoski and Carroll employed the Eulerian formulation to model steady-state orthogonal cutting [19]. This model calculated the heat generated by friction and plastic deformation. Another Eulerian model developed by Strenkowski and Moon in 1990 was capable of predicting the tool-chip contact length as well as the temperature distributions in the workpiece, chip, and tool [20].

In 1990, Shih developed an orthogonal cutting model which included the effects of sticking-sliding friction, strain rate, and heat generation [21]. This model utilized an element separation criterion based on the distance between the tip of the tool and the nodes of the workpiece. Similar models were later used to study the effects of worn tools and varying rake angles [22, 23]. In addition to the work of Shih and Strenkowski, similar orthogonal cutting models have been developed by other researchers [24-28].

When the Lagrangian formulation is used, it is necessary to define a criterion for separation of the chip from the workpiece. As a result, the development of a realistic separation criterion is an important

issue in finite element modeling of metal cutting. Several researchers have focused on this issue. Huang and Black studied the effects of using physical and geometric separation criteria of varying magnitudes [29]. They concluded that a combination of geometric and physical criteria provided the most realistic simulation of metal cutting. Zhang and Bagchi recommended a geometric criterion where the ratio of the separation distance to the depth of cut was equal to 0.05 [30]. Marusich and Ortiz used continuous remeshing along with a fracture criterion to simulate chip separation [31]. In this model, the workpiece was allowed to soften and flow around the tool, only fracturing when the criterion was satisfied. As a result, there was no need for the predefined separation line common in most finite element models.

1.6 Research Approach

1.6.1 FEM

For this thesis, finite element models of the chip formation process were developed for several metal cutting situations. These simulations were performed using a version of the FEM code DYNA3D licensed for research and education [32]. DYNA3D is an explicit, nonlinear, finite element code intended for analysis of the transient dynamic response of three-dimensional structures. It has the ability to model complex material behavior such as plasticity, rate dependence, thermal effects, and friction between surfaces in contact. Details on creating models and running simulations with DYNA3D are available in the appendix.

A model representative of those used in this work is shown in Figure 3.2. All movement is constrained to the x and y directions since orthogonal cutting may be represented by a 2 dimensional cross-section. The left and bottom faces of the workpiece were held stationary, and a constant velocity in the negative x direction was defined for the tool. In this study, the tool was considered to be rigid. Since the deformation of the tool was ignored, it was modeled with a small number of elements.

The updated Lagrangian formulation is used for the FEM simulations in this work. With the Lagrangian formulation it is necessary to specify the line where the chip will separate from the workpiece. The model is defined so that the elements will separate along the line a-b. Region 1 will form the chip, and Region 2 will form the finished surface of the workpiece. Sliding surfaces are defined to allow different parts of the model to come into contact.

Several types of sliding surfaces are available in DYNA3D for modeling contact between objects. The *sliding with separation and friction* slide surface (called a type 3 slide surface in DYNA3D) is a general surface applicable to most situations. With this surface, the specified elements are free to come

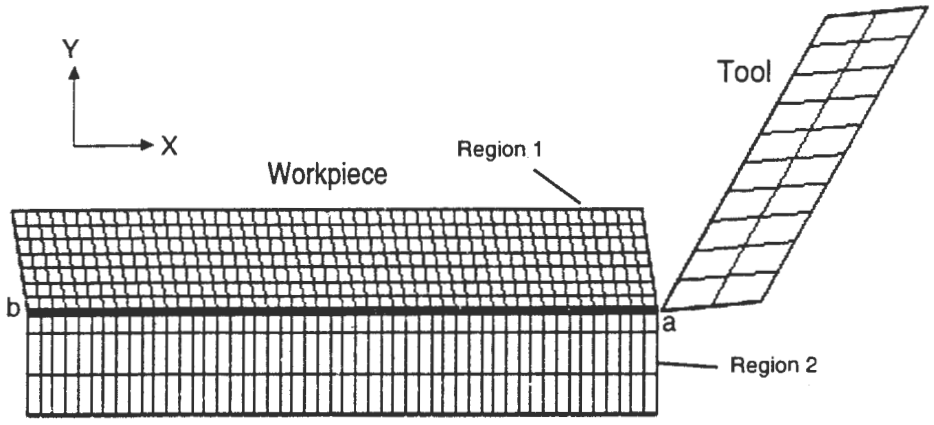

Figure 1.5 Representative finite element model

into contact or separate from each other. The contacting surfaces of the tool and chip, as well as the finished surface of the workpiece were modeled with a type 3 slide surface in order to model the friction between the surfaces. Friction between the elements is modeled as Coulombic. A constant coefficient of friction was used for this research work.

Since the elements that form the chip must be allowed to separate from the original workpiece, another type of slide surface was needed. The *tied with failure* slide surface (called a type 9 slide surface in DYNA3D) ties elements together until a specified failure criterion is satisfied. After failure occurs at a node, the surface acts as a type3 slide surface. In DYNA3D, failure is considered to occur when the following condition is met:

$$\left(\frac{F_n}{F_{nf}}\right)^2 + \left(\frac{F_s}{F_{sf}}\right)^2 \geq 1 \tag{1.2}$$

where F_n and F_s are the total normal and shear forces acting on the segment, and F_{nf} and F_{ns} are the normal and shear failure forces of the segment. The normal and shear forces are computed internally based on the segment area, and the normal and shear failure stresses are specified by the user.

The method used to model the separation of the chip from the workpiece is an important consideration. For the simulations in this work, a geometric failure criterion was added by Thean [33] to the physical failure criterion included in the original DYNA3D code. The node connecting the chip to the workpiece will separate when the condition in equation 1.2 is satisfied, or when the distance d between the node and the tip of the tool is less than 10 percent of the element length L. This is illustrated in Figure 1.6.

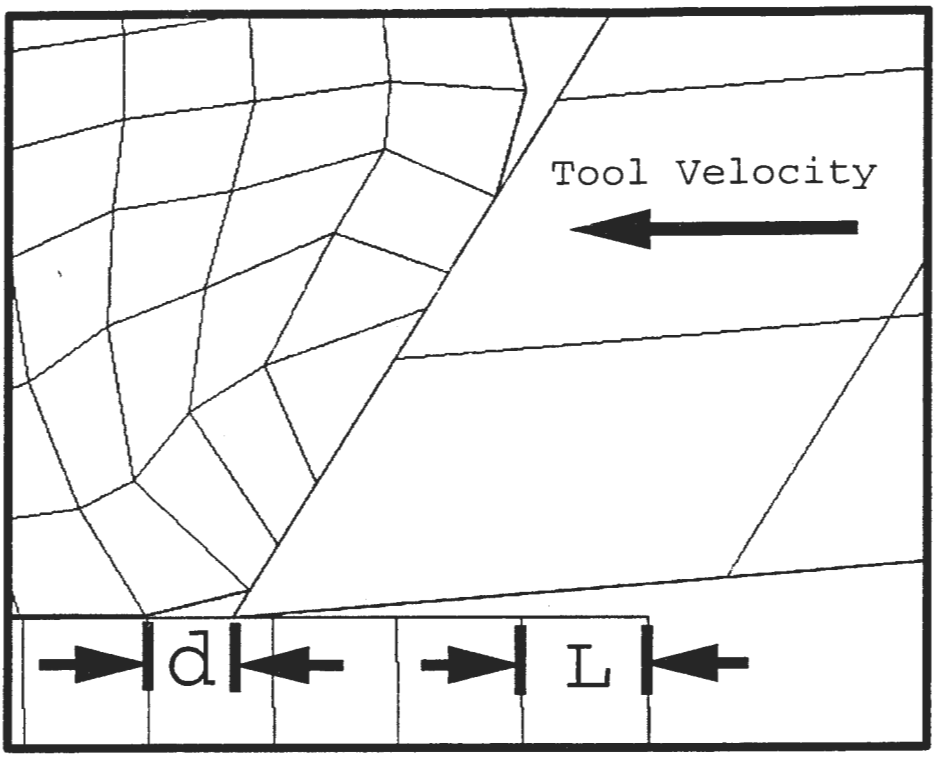

Figure 1.6 Geometric separation criterion

1.6.2 Constitutive Modeling of Material Properties

One of the most important considerations in the development of a machining simulation is the modeling of the mechanical properties of the materials used. The metal cutting process generally involves large strains and strain rates which can have a hardening effect on the chip. High temperatures are also encountered during cutting due to the plastic deformation in the workpiece and the friction between the tool and chip. All of these factors must be considered in order to produce an entirely accurate model of the machining process.

For the study detailed in the first paper, the workpiece material is modeled with a power law strain hardening relationship. In this model, the stress-strain curve is given by the following equation:

$$\sigma = K\epsilon^n \tag{1.3}$$

where the strength coefficient, K, and the strain hardening exponent, n, are properties specific to the material.

The power law strain hardening model is a simplified model that does not account for the effects of

strain rate or thermal softening. Although this model will not model the cutting process with complete accuracy, it is believed to be sufficient for the first study. The intent of the first study is to determine the effects of groove geometry on chip formation. The addition of strain rate and thermal effects to the model would have changed the magnitudes of the stresses and strains calculated in the simulation, but it is believed that the same general trends which are discussed in the conclusions would still hold true.

The work detailed in the second paper represents an advancement of the simulation model. In this paper, the mechanical properties of the workpiece are modeled with the Johnson-Cook constitutive model [34]. This model adds the effects of strain rate and thermal softening to the power law strain hardening model. In the Johnson-Cook model, the stress-strain curve is given by the following equation:

$$\sigma = [A + B(\bar{\epsilon}^p)^n][1 + Cln(\frac{\bar{\epsilon}^p}{\dot{\epsilon}_0})][1 - (\frac{T - T_r}{T_m - T_r})^m] \tag{1.4}$$

where $\bar{\epsilon}^p$ is the effective plastic strain, $\dot{\epsilon}_0$ is the reference strain rate, T is the temperature in the material, T_m is the melting temperature of the material, T_r is the room temperature, and A, B, C, n, and m are material dependent constants.

1.6.3 Experimental Validation

Validation of the simulations developed in this work was achieved through comparisons with experimental observations. These observations include machining characteristics such as the cutting forces and the shear plane angle. Forces may be measured during the cutting process with the aid of a dynamometer, and the shear plane angle may be calculated from the depth of cut and the measured thickness of the chip. Simulated results were compared to experimental results in order to show the degree of accuracy of the simulation and determine issues that should be addressed in future work.

Bibliography

[1] Ernst, H., Merchant, M.E., 1941, "Chip Formation, Friction and Finish," *Cincinnati Milling Machine Company*, Cincinnati, Ohio.

[2] Lee, E.H., Schaffer, B.W., 1951,"The Theory of Plasticity Applied to a Problem of Machining," ASME *Journal of Applied Mechanics*, Vol. 18, pp. 405-413.

[3] Rowe, G.W., Spick, P.T., 1967, "A New Approach to Determination of the Shear Plane Angle in Machining," ASME *Journal of Engineering for Industry*, Vol. 89, pp. 530-538.

[4] Wright, P.K., 1982, "Predicting the Shear Plane Angle in Machining From Workmaterial Strain-hardening Characteristics," ASME *Journal of Engineering for Industry*, Vol. 104, pp. 285-292.

[5] Stephenson, D.A., Agapiou, J.S., 1997, *Metal Cutting Theory and Practice*, Marcel Dekker Inc., New York.

[6] Lepi, S.M., 1998, *Practical Guide to Finite Elements*, Marcel Dekker Inc., New York.

[7] Spyrakos, C.C., 1994, *Finite Element Modeling in Engineering Practice*, West Virginia University Press, Morgantown, WV.

[8] Reddy, J.N., 1993, *An Introduction to the Finite Element Method*, McGraw-Hill, Inc.

[9] Nakayama, K., 1984, "Chip Control in Metal Cutting," *Bulletin JSPE*, Vol. 18, No. 2, pp. 97-103.

[10] Nakayama, K., 1962, "Chip Curl in Metal Cutting Process," Yokahama National University *Bulletin of the Faculty of Engineering*, Vol. 11.

[11] Jawahir, I. S., 1990, "On the Controllability of Chip Breaking Cycles and Modes of Chip Breaking in Metal Machining," *Annals of the CIRP*, Vol. 39, pp. 47-51.

[12] Jawahir, I.S., Zhang, J.P., 1995, "An Analysis of Chip Curl Development, Chip Deformation and Chip Breaking in Orthogonal Machining," *Trans. NAMRI/SME*, Vol. XXIII, pp. 109-114.

[13] Fang, X.D., and Jawahir, I.S., 1996, "An Analytical Model for Cyclic Chip Formation in 2-D Machining with Chip Breaking," *Annals of the CIRP*, Vol. 45, pp. 53-58.

[14] Sasahara, H., Obikawa, T., Shirakashi, T., 1993, "FEM Analysis on Three Dimensional Cutting," *J. Jap. Soc. Prec. Eng.*, Vol. 59, No. 8.

[15] Maekawa, K., Nagayama, T., Ohshima, I., Murata, R., 1990, "Finite Element Simulation of Oblique Cutting," *J. Jap. Soc. Prec. Eng.*, Vol. 24, No. 3.

[16] Klamecki, B.E., 1973, "Incipient Chip Formation in Metal Cutting - A Three-Dimension Finite Element Analysis," Ph.D. dissertation, University of Illinois at Urbana-Champaign.

[17] Tay, A.O, Stevenson, M.G., de Vahl. Davis G., 1974, "Using the Finite Element Method to Determine Temperature Distributions in Orthogonal Machining," *Proceedings of the Institute of Mechanical Engineers*, Vol. 188, pp. 627-638.

[18] Strenkowski, J.S., Carroll, J.T., 1985, "A Finite Element Model of Orthogonal Metal Cutting," *ASME Journal of Engineering for Industry*, Vol. 107, pp. 349-354.

[19] Strenkowski, J.S., Carroll, J.T., 1986, "An Orthogonal Metal Cutting Model Based on an Eulerian Finite Element Method," *Manufacturing Processes, Machines and Systems*, Proceedings of the 13th Conference on Production Research and Technology, Society of Manufacturing Engineers, Dearborn, MI, pp. 262-264.

[20] Strenkowski, J.S., Moon, K., 1990, "Finite Element Prediction of Chip Geometry and Tool/Workpiece Temperature Distributions in Orthogonal Metal Cutting," *Journal of Engineering for Industry*, Vol. 112, pp. 313-318.

[21] Shih, A.J.M., Chandrasekar, S., Yang, H.T.Y., 1990, "Finite Element Simulation of Metal Cutting Process with Strain-Rate and Temperature Effects," *Fundamental Issues in Machining*, ASME Publication PED — Vol. 43, New York, N.Y., pp. 11-24.

[22] Shih. A.J., 1995, "Finite Element Simulation of Orthogonal Metal Cutting," *ASME Journal of Engineering for Industry*, Vol. 117, pp. 84-93.

[23] Shih, A.J., 1996, "Finite Element Analysis of The Rake Angle Effects in Orthogonal Metal Cutting," *Int. Jour. Mech. Sci.*, Vol. 38, pp. 1-17.

[24] Komvopoulos, K., Erpenbeck, S.A., 1991, "Finite Element Modeling of Orthogonal Metal Cutting," *ASME Journal of Engineering for Industry*, Vol. 113, pp. 253-267.

[25] Zhang, B., Bagchi, A., 1994, "Finite Element Simulation of Chip Formation and Comparison with Machining Experiment," *ASME Journal of Engineering for Industry*, Vol. 116, pp. 289-297.

[26] Lin, Z.C., Pan, W.C., Lo, S.P., 1995, "A Study of Orthogonal Cutting with Tool Flank Wear and Sticking Behavior on the Chip-Tool Interface," *Journal of Materials Processing Technology*, Vol. 52, pp. 524-538.

[27] Eldridge, K.F., Dillon, O.W., Lu, W., 1991, "Thermo-Viscoplastic Finite Element Modeling of Machining Under Various Cutting Conditions," *Transactions of NAMRI/SME*, pp. 162-169.

[28] Kim, K.W., Sin, H., 1995, "Development of a Thermo-Viscoplastic Cutting Model Using Finite Element Method," *International Journal of Machine Tools Manufacturing*, Vol. 36, No. 3, pp. 379-397.

[29] Huang, J.M., Black, J.T., 1996, "An Evaluation of Chip Separation Criteria for the FEM Simulation of Machining," *Journal of Manufacturing Science and Engineering*, Vol. 118, pp. 545-554.

[30] Zhang, B., Bagchi, A., 1994, "A Study of Chip Separation and Its Approximation in Finite element Simulation of Continuous chip Formation," *The Physics of Machining Processes - II* , ASME Minerals, Metals & Materials Soc., p. 157.

[31] Marusich, T.D., Ortiz, M., 1995, "A Finite Element Study of Chip Formation in High-Speed Machining," ASME *Journal of Manufacturing Science and Engineering*, Vol. 3-1, pp. 245-258.

[32] Whirley, R.G., Engelmann, B.E., 1993, "DYNA3D: A Nonlinear, Explicit, Three-Dimensional Finite Element Code For Solid and Structural Mechanics – User Manual," *Lawrence Livermore National Laboratory Report UCRL-MA-10752.*

[33] Thean, W.K., McClain, B., Maldonado, G.I., Fang, X.D., 1999, "Finite Element Analysis of Chip Formation in Grooved Tool Metal Cutting," under review by the *Journal of Machining Sciences and Technology.*

[34] Johnson, G.R., Cook, W.H., 1983, "A Constitutive Model and Data for Metals Subjected to Large Strains, High Strain Rates, and High Temperatures," *Proceedings of the Seventh International Symposium on Ballistics*, the Hague, The Netherlands.

2 FINITE ELEMENT ANALYSIS OF CHIP FORMATION IN GROOVED TOOL METAL CUTTING

A paper submitted to the Journal of Machining Science and Technology

Wooi K. Thean, B. McClain, G. Ivan Maldonado, and X. D. Fang

Abstract

This paper presents the simulation of chip formation in grooved tool cutting using DYNA3D, a 3-D FEM software for dynamic nonlinear analysis which was used to simulate the orthogonal cutting problem. First, a flat face cutting tool was employed in the simulation to verify the validity of the FEM model. Next, the same simulation techniques were used to study the effects of different groove geometries on the chip formation process in orthogonal cutting. In the first set of grooved tool simulations, the depth of the groove was constant while the width was decreased. In the second set, the width was constant and the depth was increased. After analyzing the chip flow, chip curl, chip thickness, stress and strain in the chip, the effects of different groove widths and depths on the chip formation process were then discussed.

2.1 Introduction

Chip control is an important issue in machining operations that is closely tied to the prediction of chip breakability. This is particularly true in the machining of ductile materials which tend to create long chips that can become entangled in the machine, thus potentially causing delays in production and also compromising the safety of the operator. Therefore, effective chip control entails the breaking of chips to prevent the formation of long, continuous chips, and the removal of the chips to prevent damage to the machined parts. One popular method of chip breaking is to use a grooved tool in the form of a tool insert. The groove will curl the chip and direct it to break against the workpiece. In order to determine the effectiveness of a particular groove parameter, it is important to analyze the chip formation process. Such analysis provides information on the degree of chip curling, chip thickness,

chip velocity, tool-chip contact length, the forces and strains experienced by the chip, etc., all of which are parameters that could help to predict chip breaking.

Several studies on chip control and chip breaking have been published to date [1-13]. These studies have been primarily analytical or semi-analytical in nature, thus, they have relied upon empirical data obtained from extensive experiments. Numerical methods have also been employed in the field of metal cutting, of which the most popular is the finite element method (FEM). Although FEM has not been used to analyze chip breaking, it has been extensively used to study the chip formation process. Research dealing with various aspects of the FEM technique in cutting simulation, including the effects of varying cutting parameters, and the setup aspects of an FEM-based cutting model are readily found in the literature [14-23]

The objective of this study is to present an FEM simulation of the chip formation process in grooved tool metal cutting. The effects of different widths and depths of the groove geometry upon the chip's flow, curl, thickness, and stress and strain distributions are analyzed.

2.2 FEM Modeling Technique

The updated Lagrangian formulation is the choice of most FEM machining simulations because of its ability to handle kinematic nonlinear effects due to large deformations and large strains inherent to metal cutting analysis. However, its most important advantages are its ability to predict the chip's shape and to allow the actual simulation of the chip formation process from incipient to steady state cutting. In this formulation, the time variable is used as a convenient way to describe the loading and motion of a body. The aim is to evaluate the equilibrium position of the complete body at each of the discrete time points. After each time step evaluation, the body is updated from its previous equilibrium position to a new equilibrium position. The final result is obtained when the final configuration of the body is solved for the final time step. More details on this subject are available in the literature [24].

The metal cutting simulation in this research was carried out using DYNA3D [25], FEM software designed for dynamic analysis and capable of handling general contact problems. DYNA3D uses the updated Lagrangian formulation. The software allows several slide surfaces (contact interfaces) that are useful to simulate the chip formation process. The first type of DYNA3D slide surface applicable to this study is the *sliding with separation and friction* slide surface (type 3), which is capable of modeling the interface contact between the chip and the tool face because it allows two bodies to come into contact or separate in any arbitrary fashion. The user can also define Coulombic friction between the sliding surfaces based on the following equation [25]:

$$\mu = \mu_k + (\mu_s - \mu_k)e^{-\beta v_{rel}} \tag{2.1}$$

where μ_s and μ_k represent the static and kinetic friction coefficients, β is a coefficient governing the rate of change from static to kinetic friction, and v_{rel} is the relative velocity between the sliding surfaces. A second type of DYNA3D slide surface was used to simulate the chip separation process. The *tied with failure* slide surface (type 9) ties two slide surfaces together until the following criterion is satisfied [25]:

$$\left(\frac{F_n}{F_{nf}}\right)^2 + \left(\frac{F_s}{F_{sf}}\right)^2 \geq 1 \tag{2.2}$$

where F_n and F_s are the total normal and shear forces acting on the segment, and F_{nf} and F_{ns} are the normal and shear failure forces of the segment. The normal and shear forces are computed internally based on the segment area, and the normal and shear failure stresses are specified by the user.

A slide surface is created when the user defines one master surface and one slave surface on the elements' faces where interfacial contact will take place. Through the penalty method, the slave surface is not allowed to penetrate the master surface. When excessive element penetration is detected, a restoring force is calculated that restores the penetrating node to within a specified degree of penetration.

The first simulation in this study was performed to verify the validity of the FEM model relative to the results obtained by Black and Huang [23]. Therefore, the same cutting parameters, material properties and simulation techniques as used by Black and Huang were adapted into this simulation. A flat face tool was used to simulate an orthogonal cutting problem. Although DYNA3D is designed for 3-D analysis, the model was restricted to approximate plane-strain conditions so that the tool and workpiece material could move only in the x and y direction. This was achieved by defining two symmetry planes on the two surfaces of the model perpendicular to the z-axis. The symmetry planes will restrict elemental movement in the z-axis direction.

Before conducting any tests, a mesh refinement study was undertaken in order to determine the mesh density necessary to produce accurate results. Identical tests were conducted with the workpiece divided into 500, 1200, and 2000 elements. A comparison of the three trials showed little change in the effective stress contours, with only a slight increase in the maximum values. The maximum effective stress value was 2.9 percent higher for the case with 1200 elements and 4.8 percent higher for the case with 2000 elements. Since increasing the mesh density significantly increased the computation time and produced only minimal changes in the results, the original mesh was deemed adequate and a workpiece consisting of 500 elements and a tool consisting of 12 elements was chosen.

The workpiece was modeled with an isotropic elastic-plastic material with power law strain hardening. The properties of SAE 1112 steel were used with the modulus of elasticity at 207 GPa and Poisson's ratio at 0.29. The stress-strain curve of the material was obtained from Oxley [26] and is shown in Figure 2.1. The effects of strain rate hardening and thermal softening have been ignored for this study. The tool material was modeled as perfectly elastic. Since tool wear was not considered in this study and the tool material was assumed to be much stiffer than the workpiece, the modulus of elasticity of the tool was arbitrarily set to be four times larger than that of the workpiece. The cutting tool edge was assumed to be perfectly sharp and a rake angle of 30 degrees was used. Both the workpiece and tool were composed of eight-node solid elements (brick elements).

To simulate cutting, the tool was assumed to move in the negative x direction and the workpiece was assumed to be stationary. Tool motion was modeled by prescribing a velocity of 263 mm/s. Constraints were placed on the tool so that no movement was allowed in the y or z directions. Constraints were also placed on the left face and bottom face of the workpiece so that no movement was allowed in any direction. A clearance was also provided at the tool flank with a clearance angle of 5 degrees. Figure 2.2a provides a schematic of the simulation.

During the cutting process, the tool penetrates into the workpiece and scrapes away the unwanted material. When the chip (segment A) separates from the workpiece, it comes into contact with the tool-chip interface c-d. To simulate the chip sliding along this interface without penetrating into the tool material, a contact surface must be defined, so the type 3 slide surface was used. Interface c-d was defined as the master surface and interface a-b of segment A was defined as the slave surface. Between the two slide surfaces, a simple static friction coefficient based on Coulombic friction was employed. This was achieved with the built-in frictional condition shown in Equation 2.1. By specifying μ_k and β to be zero, a rate-independent friction model is obtained with $\mu = \mu_s$. A friction coefficient of 0.1 was chosen for the final simulation. Based on the work of Komvopoulos and Erpenbeck [18], a low friction coefficient may be representative of well lubricated interfaces.

In order to simulate the chip separation, segment A must be allowed to separate from segment B in the workpiece when a separation criterion is met. This is achieved by prescribing the type 9 slide surface on the predefined chip separation line a-c. Huang and Black [23] conducted an extensive study on the geometrical and physical chip separation criteria, the two types of chip separation criteria commonly used in FEM machining simulation. Since the intent of this study was to simulate the chip formation process from incipient to steady state cutting, the chip separation criterion was adapted from the algorithm suggested by [23], namely a combination of the geometrical and physical criteria. The

physical criterion is based on Equation 2.2. The geometrical criterion is based on the distance between the tool tip and the immediate separating node ahead of the tool tip. When this distance is less than a critical value, the criterion is satisfied and the nodes joining Segment A and Segment B will separate. In most machining studies conducted where the geometrical criterion was used, the critical distance was found from trial and error. Zhang and Bagchi [20] suggested that the value should be approximately 10 to 30 percent of the workpiece elemental length. In this study, the value of this distance was obtained from several trial runs with the value set between zero to 30 percent of the workpiece elemental length. It was observed that at less than 10 percent, the finite element mesh suffered large distortion. When the value was set between 10 to 30 percent, the numerical stability improved and the analysis time also decreased. However, when the value increased from 10 to 30 percent, the size of the crack ahead of the tool tip also increased. In actual cutting of ductile material, this crack is not formed in steady state cutting. Thus, the critical value of this study was chosen at 10 percent of the elemental length so that the crack is minimized but not at the expense of severe elemental distortion.

The effective stress contours corresponding to the tool's final position are shown in Figure 2.2b. The chip shape, elemental deformation and stress contours are consistent with the results obtained by Huang and Black. In fact, the maximum effective stress value of 856 MPa is nearly identical to the maximum value of 860 MPa obtained in a similar test performed by Huang and Black [23]. The higher stress region that extends from the tool tip to the free surface of the chip shows the existence of the primary deformation zone. The higher stress region at the tool/chip interface shows the secondary deformation zone. In summary, the flat face tool results provided comparable results to other works in the literature and thus adequate confidence in the methodology herein employed to encourage the pursuit of a grooved tool simulation.

2.3 Grooved Tool Simulation

A standard approach in inducing chip fracture is to direct the chip towards an obstacle, such as the unmachined workpiece surface or tool holder, to produce a bending stress for breaking. This can be achieved by using a grooved cutting tool. A grooved tool allows the chip to flow into the groove, which reduces the chip curl radius and enables the grooved tool to direct the chip more effectively into an obstacle. According to Jawahir and Zhang [12], the groove's back wall also imparts additional force to create a bending moment along the chip that promotes chip breaking. The advantage of a grooved tool chip breaker is that it requires no setup, increases the effective rake angle and reduces the tool-chip contact length [18]. This in turn reduces the required cutting forces.

Zhang [27] showed that chip control depends on the factors of chip up-curl radius, chip thickness and the properties of the work material. Nakayama [1] produced a chip breaking criterion that showed that a chip will break when the strain on the chip surface exceeds the ultimate strain of the chip material. The strain on the chip surface is calculated from the chip thickness and radius of curvature, and this relationship is given by:

$$\epsilon_B = \frac{t_2}{2}\left(\frac{1}{R_O} - \frac{1}{R_L}\right) \tag{2.3}$$

where t_2 is the thickness of the chip, R_0 is the inherent radius of curvature of the chip, and R_L is the limiting radius for the chip to miss the tool shank or any other obstacles.

The focus of this research is to use FEM to analyze how various widths and depths of a grooved tool affect the chip flow and chip curling characteristics. Techniques from the previous simulation of a flat face cutting tool were modified to analyze a grooved tool problem. First, a base test case was simulated to demonstrate the capability of DYNA3D to simulate a complete chip curl in grooved tool cutting. A groove was modeled into the cutting tool with a width of 0.75 mm and a depth of 0.14 mm. The cutting depth was 0.11 mm. Since the effective rake angle at the tool tip is now larger because of the groove, the tool's rake angle was set to 0 degrees so that a shearing process is obtained. If a rake angle of 30 degrees was used, the chip formation will imitate a peeling process rather than a shearing process. Land width was not considered in this study because modeling the land width will cause a sharp corner to exist near the leading edge of the groove that changes the slope abruptly, which in turn causes the chip elements to undergo excessive deformation when sliding into the groove, thus yielding numerical instabilities.

The chip curling pattern from the grooved tool simulation at various times is shown in Figures 2.3a through 2.3f. Examination of the figures shows the general element deformation in the deformed chip is not excessive. The chip thickness is constant throughout the length of the chip indicating that chip upward flow was not restricted in the simulation.

The results of this simulation compare favorably with experimental studies of chip formation. The chip curvature is approximately constant in the half-circle state as shown in Figure 2.3d. Although not apparent at first, a close inspection of Figure 2.3f shows that the chip has become an ear-shaped chip. The progression of the simulated chip from circular to ear-shaped closely matches the stages of chip development commonly observed in cutting experiments as shown by Jawahir and Zhang [12]. It should also be noted that the simulated chip increases in radius after impacting the workpiece. This is consistent with experimental observations of chip formation as described by both [12] and Nakayama

[2]. The close agreement between this simulation and experimental observations further validates the accuracy of the methodology employed in this study.

2.3.1 Effect of Groove Width on Chip Formation

The width and depth of a groove are important in controlling chip curl because it affects the radius of curvature of the groove. To study how various widths affect the chip formation process, three simulations were performed (simulations 1a through 3a). The same techniques and cutting parameters from the flat face tool simulation were used, and the rake angle was set to 0 degrees for the same reason previously mentioned. Three different groove sizes were modeled into the tool with their respective parameters described in Table 2.1. The final tool positions with their corresponding effective strain contours and effective stress contours are shown in Figures 2.4, 2.5 and 2.6, respectively.

Table 2.1 Groove parameters for studying the effect of different widths and depths

	GROOVE PARAMETERS	
Simulation	Width	Depth
1a	0.10 mm	0.14 mm
2a	0.09 mm	0.14 mm
3a	0.08 mm	0.14 mm
1b	0.10 mm	0.16 mm
2b	0.10 mm	0.18 mm
3b	0.10 mm	0.20 mm

In Figure 2.4, the presence of a slight gap between the chip and tool near the groove's top edge shows that the chip was not formed under the full influence of the groove. However, when the width was decreased, the groove had a greater influence upon the chip formation process. This is indicated by an increasingly smaller gap in Figure 2.5 and virtually no gap in Figure 2.6. The chip formation in Figure 2.6 was under the full influence of the groove because the chip material fully occupied the groove. Therefore, the upper half of the groove restricted the upward flow of the chip and caused chip jamming to occur at the free surface region, the region where the chip started to curl upward. Unlike Figures 2.4 and 2.5 which show fairly smooth radius of curvatures in their free surface regions, the free surface region of Figure 2.6 has a small protrusion on the surface as a result of restricted chip flow (chip jamming).

The following trends can be observed from Figures 2.4 through 2.6 when the groove width is de-

creased. Although the pattern of the strain contours may look similar, the strain magnitude increases with decreasing width. The largest effective strain magnitude is found in the simulation with the smallest width. The strain contours in the primary deformation shear zone also become more widely distributed. The chip radius along the chip/tool interface also increases and resembles the groove's radius of curvature. Since the groove depths were unchanged in the three simulations while the groove widths were reduced, the grooves' radius of curvature were increased, and similarly, the chips' radius of curvature were also increased. This may suggest that the chip radius, an indicator of chip curling, is strongly influenced by the radius of the groove.

Chip thickness also increases with decreasing groove width. As mentioned earlier, the chip upward flow is more restricted when the width is reduced due to greater influence of the groove on the chip formation process. Therefore, due to volume conservation, the material that could not be displaced vertically was displaced horizontally, thus increasing the chip thickness. The effective stress results show that the stress contours are more widely distributed in the primary deformation zone when groove width decreases. This may indicate that deformation in the primary zone occurs over a wider region. Similar to the effective strain results, the largest effective stress is found in the simulation with the smallest width.

2.3.2 Effect of Groove Depth on Chip Formation

To study the effect of various groove depths on the chip formation process, three additional simulations (simulations 1b through 3b), with the groove parameters as specified in Table 2.1, were performed. All parameters in these simulations were similar to the previous trials, except that the groove widths were fixed and the depths were increased. The final tool positions with their corresponding effective strain contours and effective stress contours are shown in Figures 2.7, 2.8 and 2.9, respectively.

In all three simulations, a small gap exists in the upper part of the chip/tool interface. This indicates that the chip formation process was not fully influenced by the groove. Even so, changes in the groove parameters cause some apparent changes in the shapes of the chips, and the stress and strain distributions within them. In fact, as the depth of the groove increases, the strain magnitude in the chip is reduced even though the strain contour patterns look similar. The effective stress magnitude also decreases with increasing depth. The largest stress and strain magnitudes are found in the simulation where the depth is smallest. The stress contours show that the highest stress region is not concentrated in a plane but rather in the free surface region. A high stress region, which also defines the primary deformation zone, is found to extend from the tool tip to the free surface region. By inspecting this

area, it is apparent that elemental deformation first began to occur when the elements approached the primary deformation zone area.

While increasing groove depth and keeping groove width constant, the groove's radius of curvature is decreased. Therefore, when the workpiece material flows into the groove to form the chip, the chip's radius of curvature is reduced along with the groove's radius of curvature. This can be observed from the chip curling patterns of Figures 2.7 through 2.9. The chip with the most curling is seen in the groove with the largest depth. Also, the simulations form thinner chips when the depth increases.

2.3.3 Localized Effective Stress and Strain Behavior

As mentioned in reference [2], the chip will break when the strain in the chip root near the free surface of the chip exceeds the ultimate strain of the chip material. In all six simulations presented, the effective strain in these regions was maximum when the chip formation reached steady state. The impact of varying groove width and depth on this localized strain versus time is shown in Figure 2.10. The corresponding localized effective (von Mises) stress versus time plot is shown in Figure 2.11. Examination of these figures shows that all test cases reached steady state by 10,000 μs except for cases 2a and 3a, which were still showing an increase in the effective strain at the chip root. From the results shown in Figure 2.10, one would expect the chip in Simulation 3a to break earliest because its effective strain is the highest at any given time beyond 1000 μs.

The localized effective strain does not appear to correlate to chip curvature. Unlike the results in Figure 2.10, the curvatures in simulation 3a to 3b do not follow a pattern. However, the chip thickness decreases from simulation 3a to 3b. Also, from Figure 2.11, the effective stress decreases from simulation 3a to 3b. Therefore, it can be concluded that the effective strain and stress in the free surface of the chip increases with the chip thickness, where larger strain and stress is found in thicker chips in grooved tool cutting before the free end of the chip touches the workpiece, similar to that in flat face tool cutting.

2.4 Conclusions

In this work, FEM simulations of the chip formation process in grooved tool metal cutting are presented. These simulations were shown to compare favorably with experimental chip formation studies in the literature [2, 12, 23]. In order to study how the groove geometry affects the chip formation process, three different groove widths and three different groove depths were simulated. The effects of width and depth on the chip formation process for a grooved tool without land were discussed based on the simulation results and are summarized below.

1. The chip's radius of curvature is significantly influenced by the radius of the groove because the chip material flows into the groove and it adopts the form of the groove. Chip curvature was observed to decrease when the groove depth was constant and the width was decreased, or when the width was constant and the depth was increased, where in both cases the radius of curvature of the groove decreases.

2. Chip thickness is affected by how quickly the effective rake angle of the groove changes from positive to negative. When the chip flows into the negative effective rake angle section of the groove, its upward flow is restricted by the groove wall. This is compensated by horizontal flow of the chip material which increases the chip thickness. However, chip thickness in grooved tool cutting is also affected by the natural curl and natural chip thickness of the chip material when a groove is not present. If the chip has a higher tendency to curl, then the restriction imposed by the negative rake face section of the groove will be less pronounced. Further research in this area should be carried out to determine the exact relationship between chip thickness and the mentioned parameters.

3. Similar to flat face tool cutting, the effective stress and strain in the chip root near the free surface of the chip increase with the chip thickness in grooved tool cutting before the free end of the chip touches the workpiece. However, chip curvatures may not affect these values prior to contact.

Although this study did not consider the effects of strain rate and thermal softening, the conclusions show consistency with other work in the field. Strain rate and thermal softening will affect the magnitude of the stresses and strains found in the chip. However, it is expected that the general trends resulting from varying groove geometries discussed in this paper will still be evident when these factors are considered. Consequently, a study of strain rate and thermal softening effects has been left for future work.

Bibliography

[1] Nakayama, K., 1962, A Study on Chip Breaking, *Bulletin of JSME*, Vol .5, No. 17 , pp. 142-150.

[2] Nakayama, K., 1984, Chip Control in Metal Cutting, *Bulletin JSPE*, Vol. 18, No. 2, pp. 97-103.

[3] Pekelharing, A.J., 1964, Why and How Does the Chip Curl and Break ?, *Annals of CIRP*, Vol. 12, pp 144-147.

[4] Spaans, C., 1970, A Systematic Approach to Three Dimensional Chip Curl, Chip Breaking and Chip Control, *SME Paper*, MR 70-241.

[5] Spaans, C., 1971, *The Fundamentals of Three Dimensional Chip Curl, Chip Breaking and Chip Control,* PhD Thesis, TH Delft, Netherlands.

[6] Spaans, C., vanGeel, P. F. H. J., 1970, Basic Mechanism Cutting with a Chip Breaker, *Annals of the CIRP*, Vol. 18, pp. 87-92.

[7] Worthington, B., Redford, A. H., 1973, Chip Curl and the Action of the Groove Type Chip Former, *Int. J. of Machine Tool Design and Research*, Vol. 13. pp. 257-270.

[8] Worthington, B., 1975, The Effect of Rake Face Configuration on the Curvature of the Chip in Metal Cutting, *Int. J. of Machine Tool Design and Research*, Vol. 15, pp. 223-239.

[9] Kaldor, S., Ber, A., Lenz, E., 1979, On the Mechanism of Chip Breaking, *Transactions of the ASME*, Vol. 101, pp. 241-249.

[10] Jawahir, I. S., 1990, On the Controllability of Chip Breaking Cycles and Modes of Chip Breaking in Metal Machining, *Annals of the CIRP*, Vol. 39, pp. 47-51.

[11] Ganapathy, B.K., Jawahir, I.S., 1993, A Force Model for Chip Breaking in Orthogonal Machining, *ASME Proc. Manuf. Sce. and Engg.*, PED Vol. 64, pp. 461-474.

[12] Jawahir, I.S., Zhang, J.P., 1995, An Analysis of Chip Curl Development, Chip Deformation and Chip Breaking in Orthogonal Machining, *Trans. NAMRI/SME*, Vol. XXIII, pp. 109-114.

[13] Fang, X.D., and Jawahir, I.S., 1996, An Analytical Model for Cyclic Chip Formation in 2-D Machining with Chip Breaking, *Annals of the CIRP*, Vol. 45, pp. 53-58.

[14] Strenkowski, J.S., Carroll, J.T., 1985, "A Finite Element Model of Orthogonal Metal Cutting," *ASME Journal of Engineering for Industry*, Vol. 107, pp. 349-354.

[15] Strenkowski, J.S., Carroll, J.T., 1986, "An Orthogonal Metal Cutting Model Based on an Eulerian Finite Element Method," *Manufacturing Processes, Machines and Systems*, Proceedings of the 13th Conference on Production Research and Technology, Society of Manufacturing Engineers, Dearborn, MI, pp. 262-264.

[16] Strenkowski, J.S, Moon, K.-J., Oct. 6-9, 1987, "An Improved Finite Element Model of Orthogonal Metal Cutting," *Manufacturing Processes, Systems and Machines*, Proceedings of 14th Conference

on Production Research and Technology, Society of Manufacturing Engineers, Dearborn, MI, pp. 67-72.

[17] Shih, A.J.M., Chandrasekar, S., Yang, H.T.Y., 1990, "Finite Element Simulation of Metal Cutting Process with Strain-Rate and Temperature Effects," *Fundamental Issues in Machining*, ASME Publication PED — Vol. 43, New York, N.Y., pp. 11-24.

[18] Komvopoulos, K., Erpenbeck, S.A., 1991, "Finite Element Modeling of Orthogonal Metal Cutting," *ASME Journal of Engineering for Industry*, Vol. 113, pp. 253-267.

[19] Zhang, B., Bagchi, A., 1994, "Finite Element Simulation of Chip Formation and Comparison with Machining Experiment," *ASME Journal of Engineering for Industry*, Vol. 116, pp. 289-297.

[20] Zhang, B., Bagchi, A., 1994, "A Study of Chip Separation and Its Approximation in Finite element Simulation of Continuous chip Formation," *The Physics of Machining Processes - II* , ASME Minerals, Metals & Materials Soc., p. 157.

[21] Shih. A.J., 1995, "Finite Element Simulation of Orthogonal Metal Cutting," *ASME Journal of Engineering for Industry*, Vol. 117, pp. 84-93.

[22] Shih, A.J., 1996, "Finite Element Analysis of The Rake Angle Effects in Orthogonal Metal Cutting," *Int. Jour. Mech. Sci.*, Vol. 38, pp. 1-17.

[23] Huang, J.M., Black, J.T., 1996, "An Evaluation of Chip Separation Criteria for the FEM Simulation of Machining," *Journal of Manufacturing Science and Engineering*, Vol. 118, pp. 545-554.

[24] Bathe, K.-J., 1996, *Finite Element Procedures*, Prentice-Hall, Inc., Englewood Cliffs, N.J.

[25] Whirley, R.G., Engelmann, B.E., 1993, "DYNA3D: A Nonlinear, Explicit, Three-Dimensional Finite Element Code For Solid and Structural Mechanics – User Manual," *Lawrence Livermore National Laboratory Report UCRL-MA-10752.*

[26] Oxley, P. L. B., 1989, *Mechanics of Machining: An Analytical Approach to Assessing Machinability,* Ellis Horwood Limited, West Sussex, England.

[27] Zhang, Y.P., 1980, "Chip curl, Chip Breaking And Chip Control of the Difficult-to-Cut Materials", *Annals of the CIRP*, pp. 79-83.

[28] Stephenson, D.A., Agapiou, J.S., 1997, *Metal Cutting Theory and Practice*, Marcel Dekker Inc., New York.

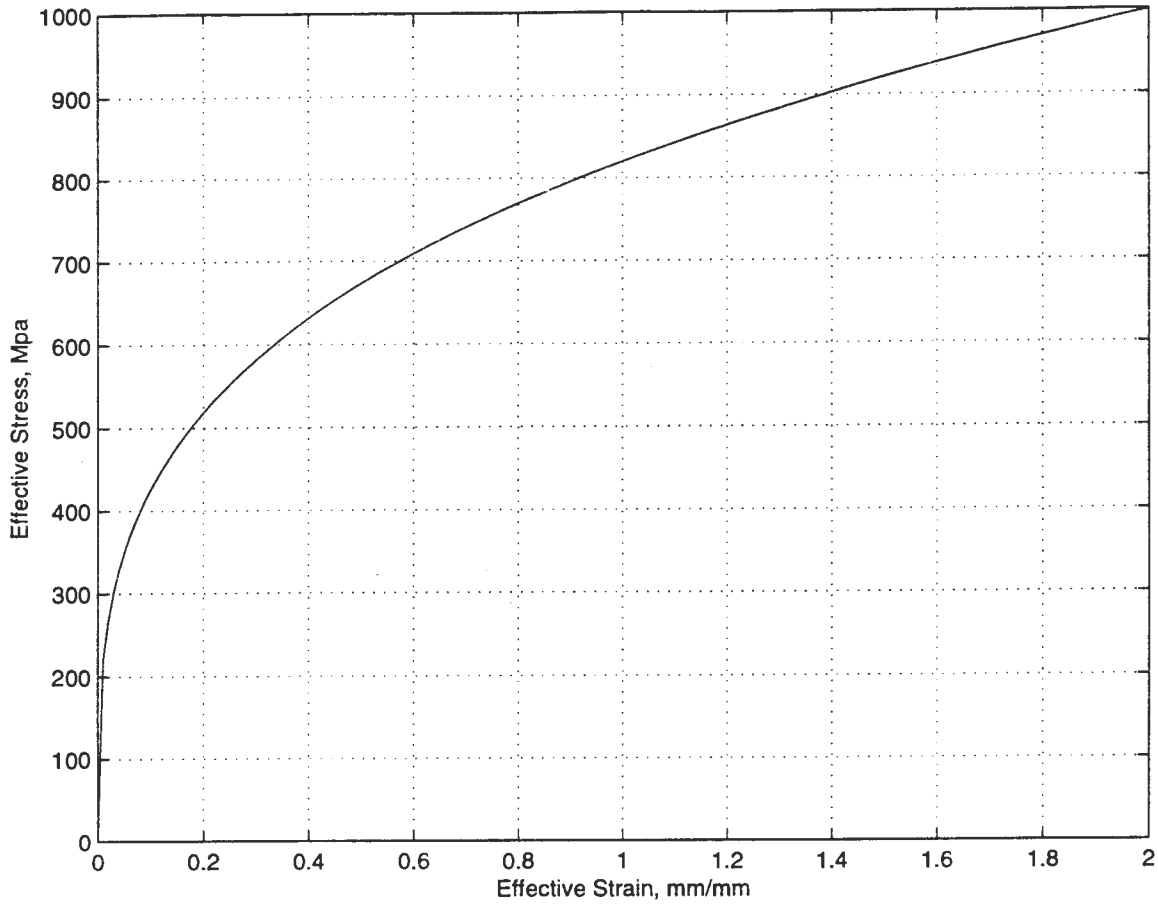

Figure 2.1 Stress-strain curve for 1112 steel

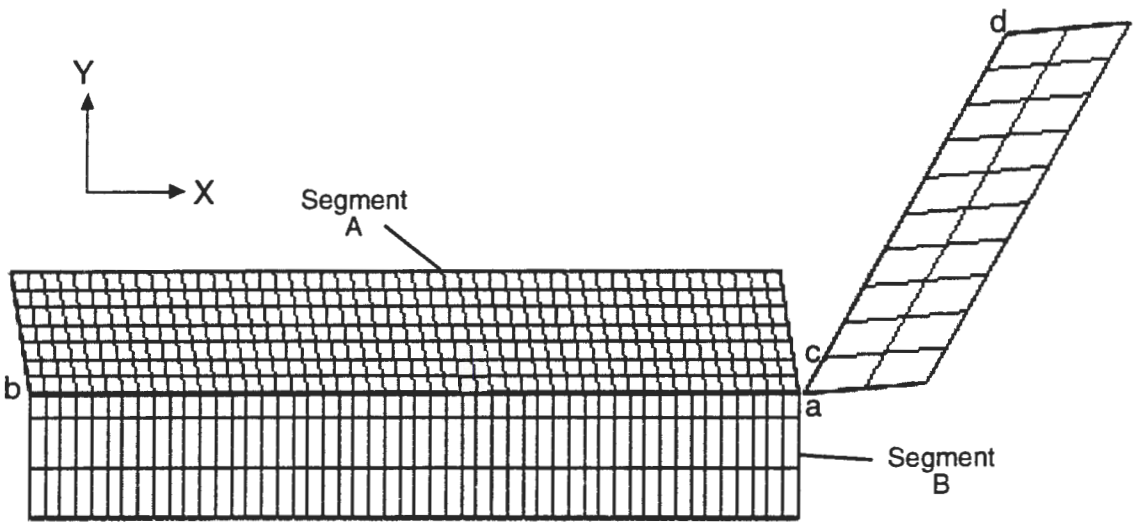

(a)

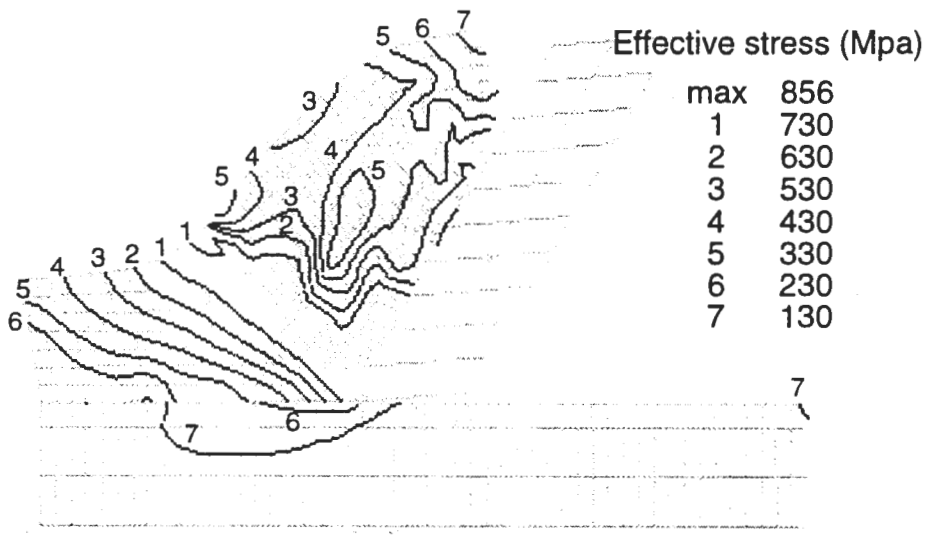

(b)

Figure 2.2 (a) setup of flat face tool model (b) effective stress contours of final tool position

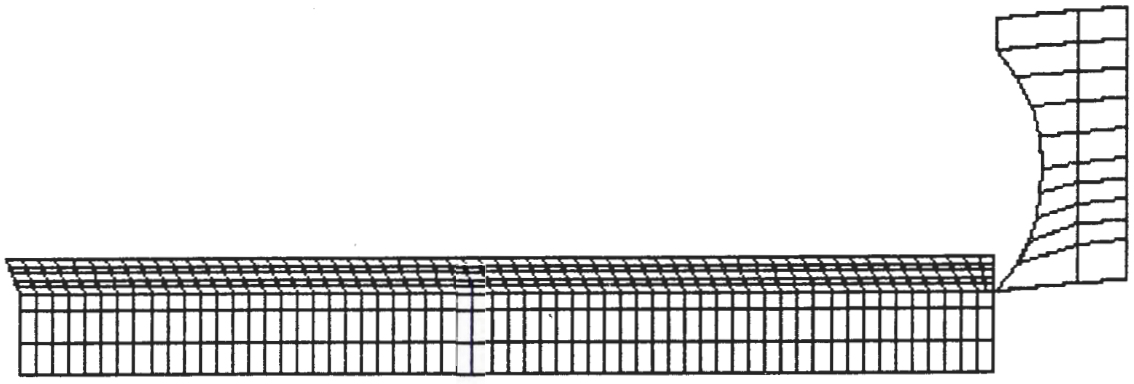

(a) t = 0.00e+00

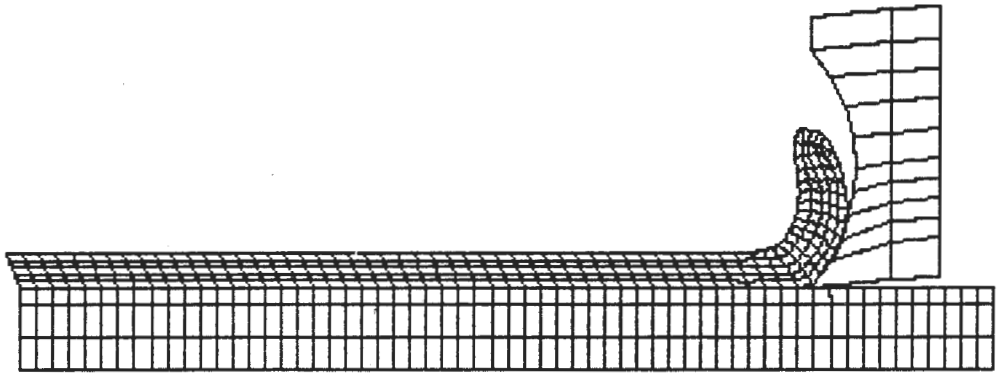

(b) t = 1.16e+03

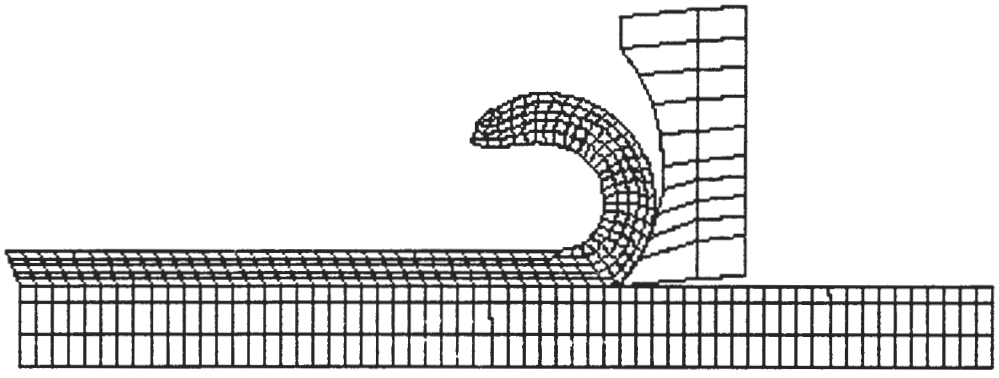

(c) t = 2.36e+03

Figure 2.3 Chip curling at various time steps (Time given in μs)

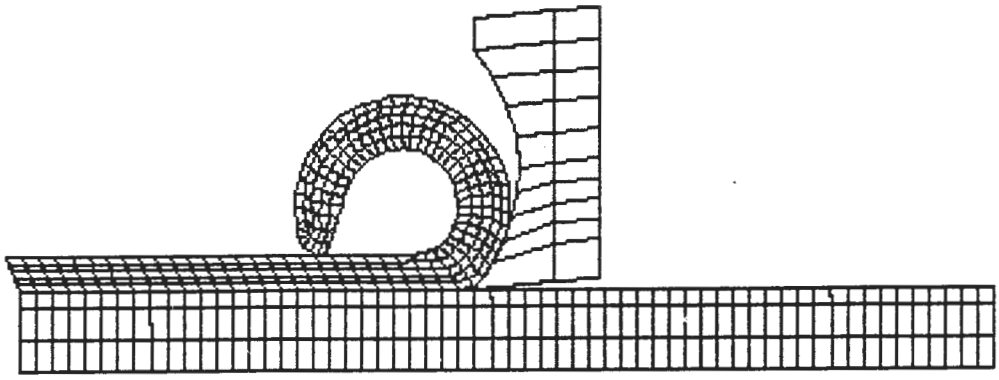

(d) t = 3.28e+03

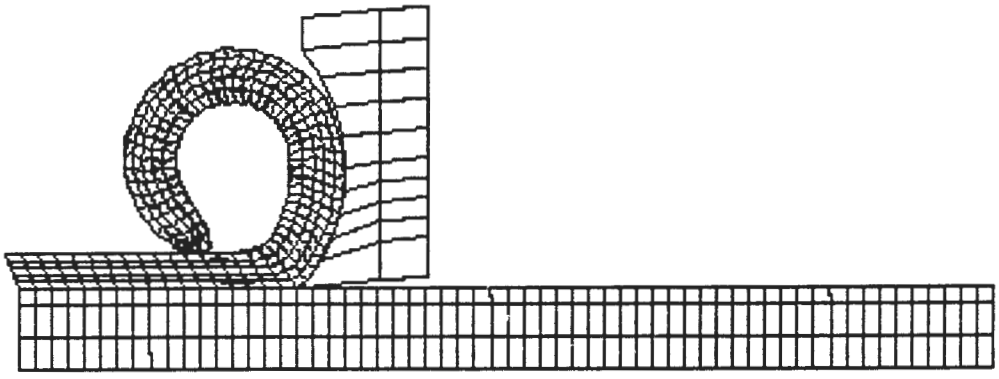

(e) t = 4.36e+03

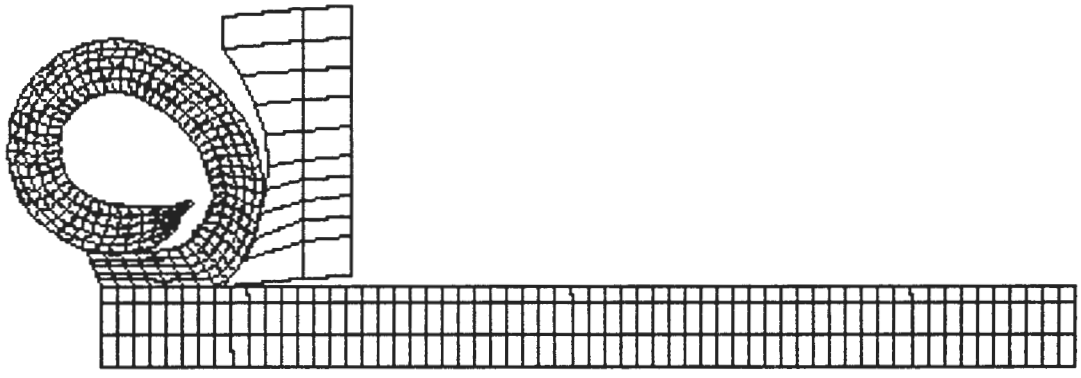

(f) t = 5.36e+03

Figure 2.3 (Continued)

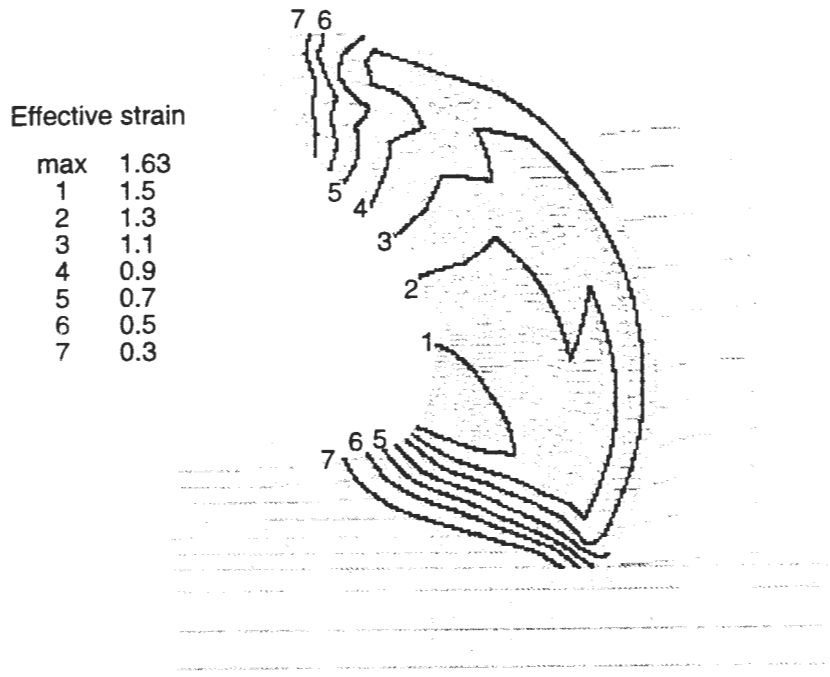

(a)

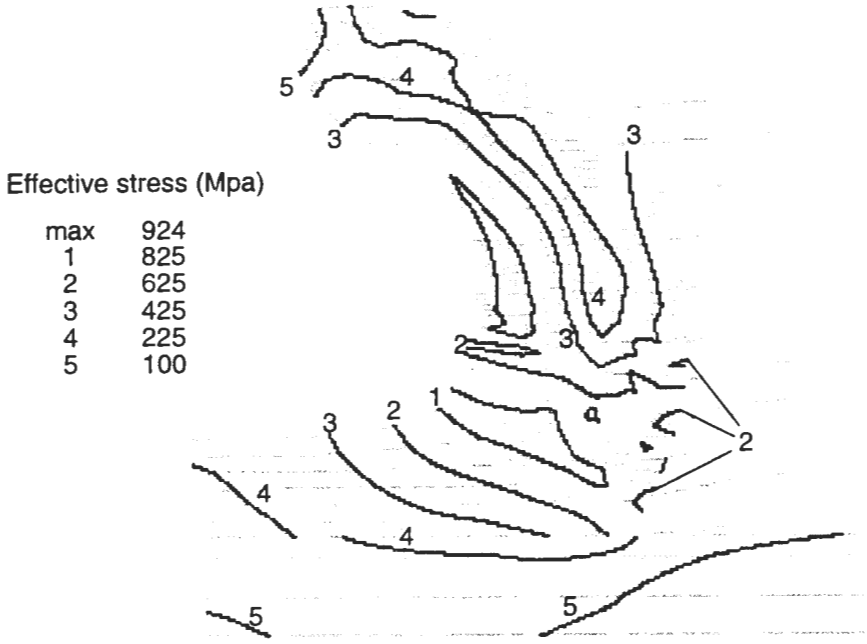

(b)

Figure 2.4 Simulation 1a: (a) effective strain contours (b) effective stress contours

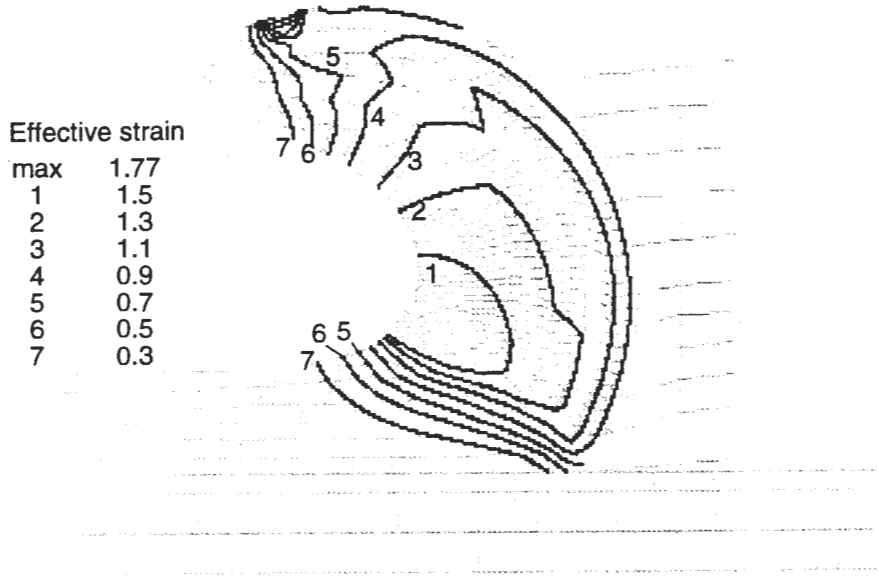

(a)

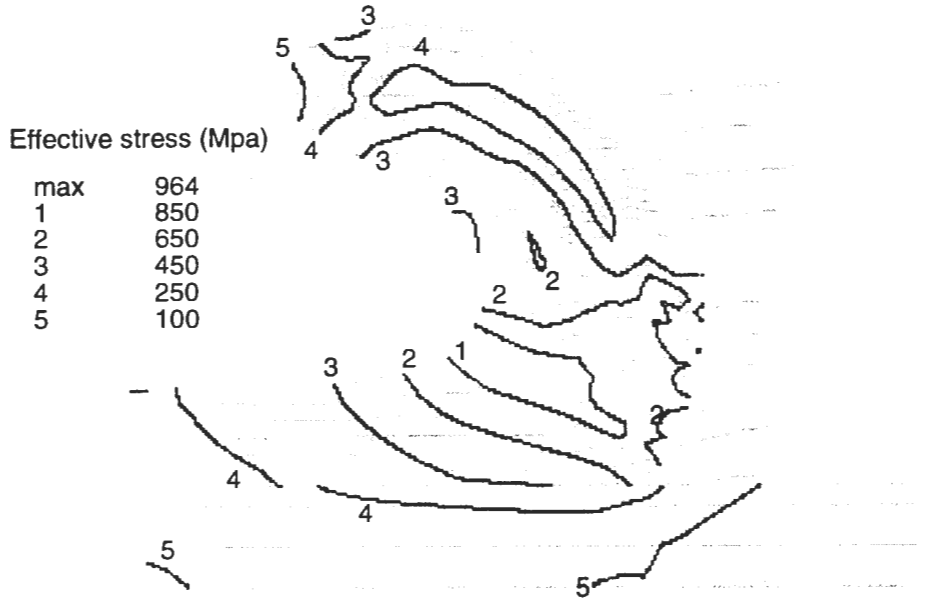

(b)

Figure 2.5 Simulation 2a: (a) effective strain contours (b) effective stress contours

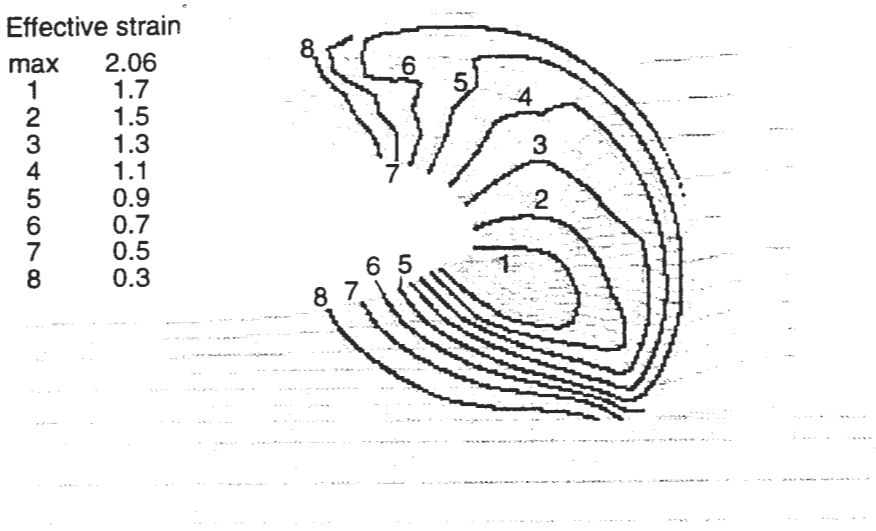

(a)

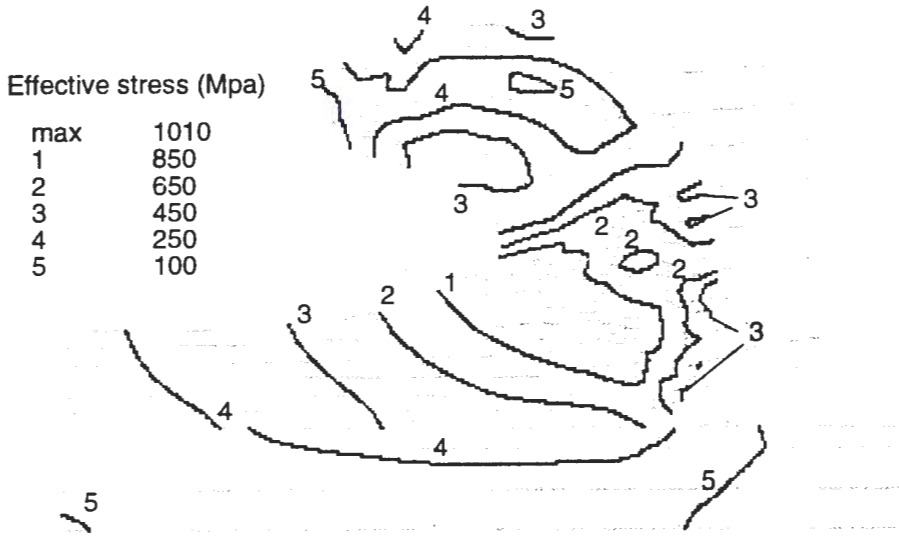

(b)

Figure 2.6 Simulation 3a: (a) effective strain contours (b) effective stress contours

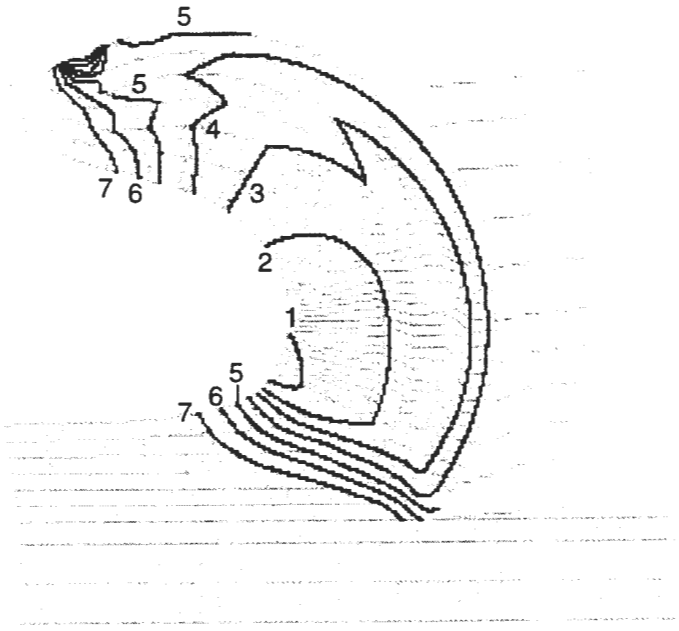

(a)

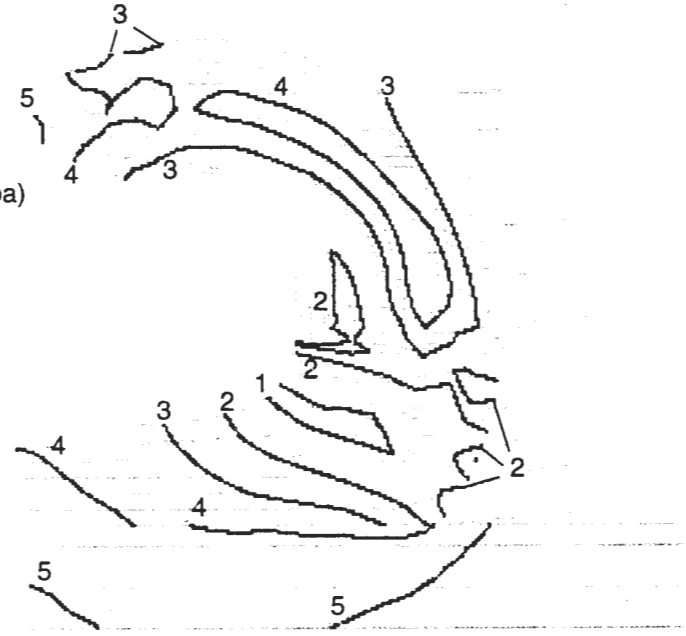

(b)

Figure 2.7 Simulation 1b: (a) effective strain contours (b) effective stress contours

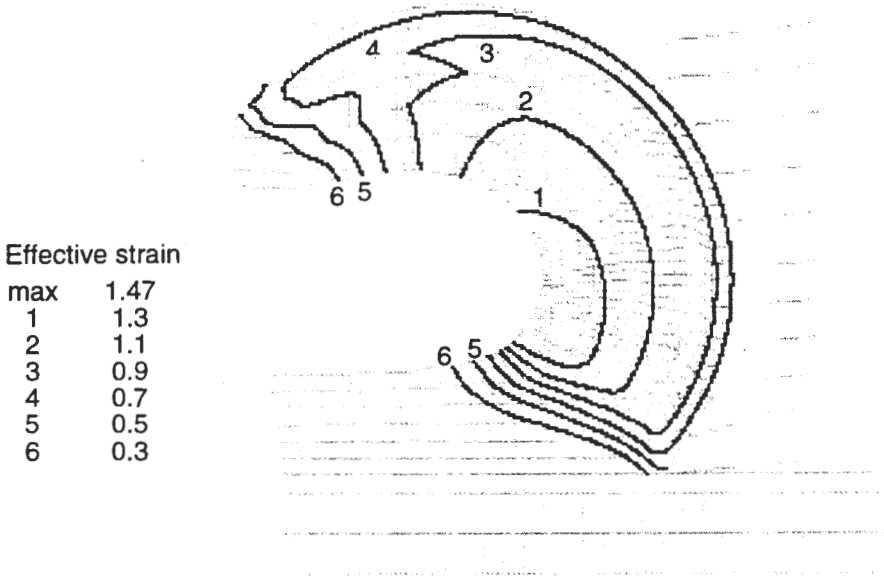

(a)

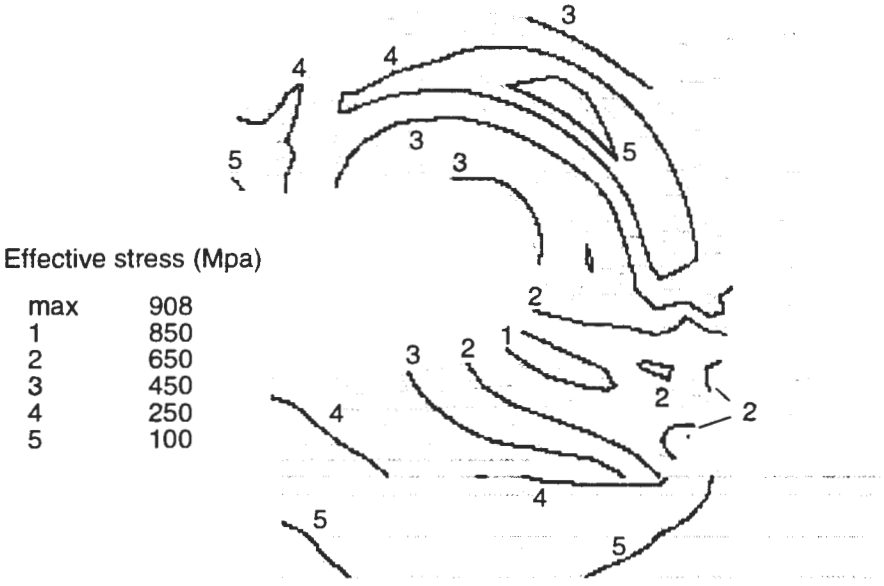

(b)

Figure 2.8 Simulation 2b: (a) effective strain contours (b) effective stress contours

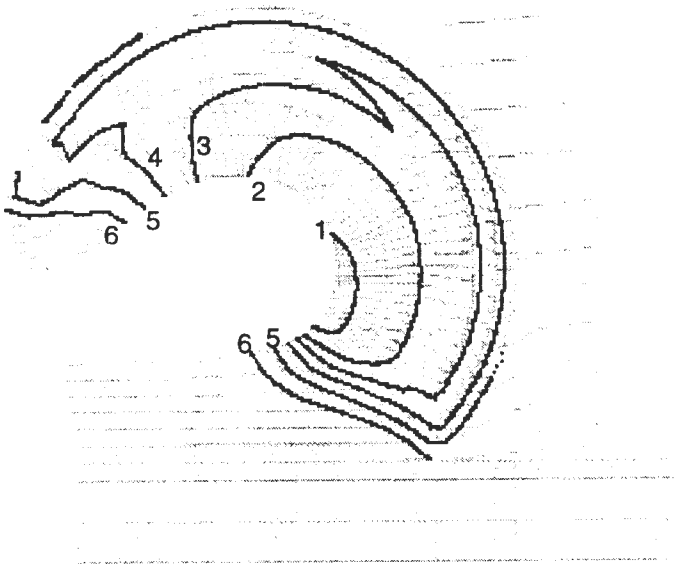

(a)

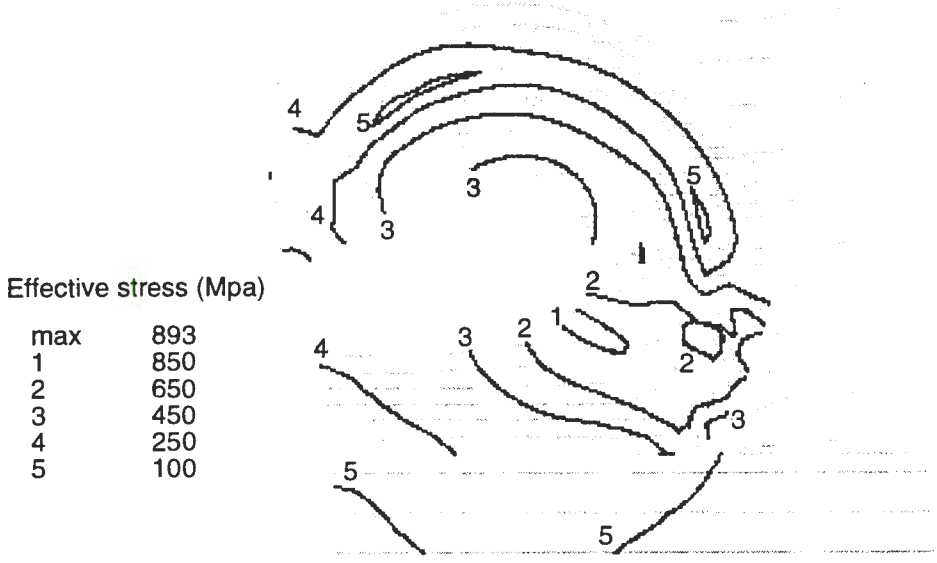

(b)

Figure 2.9 Simulation 3b: (a) effective strain contours (b) effective stress contours

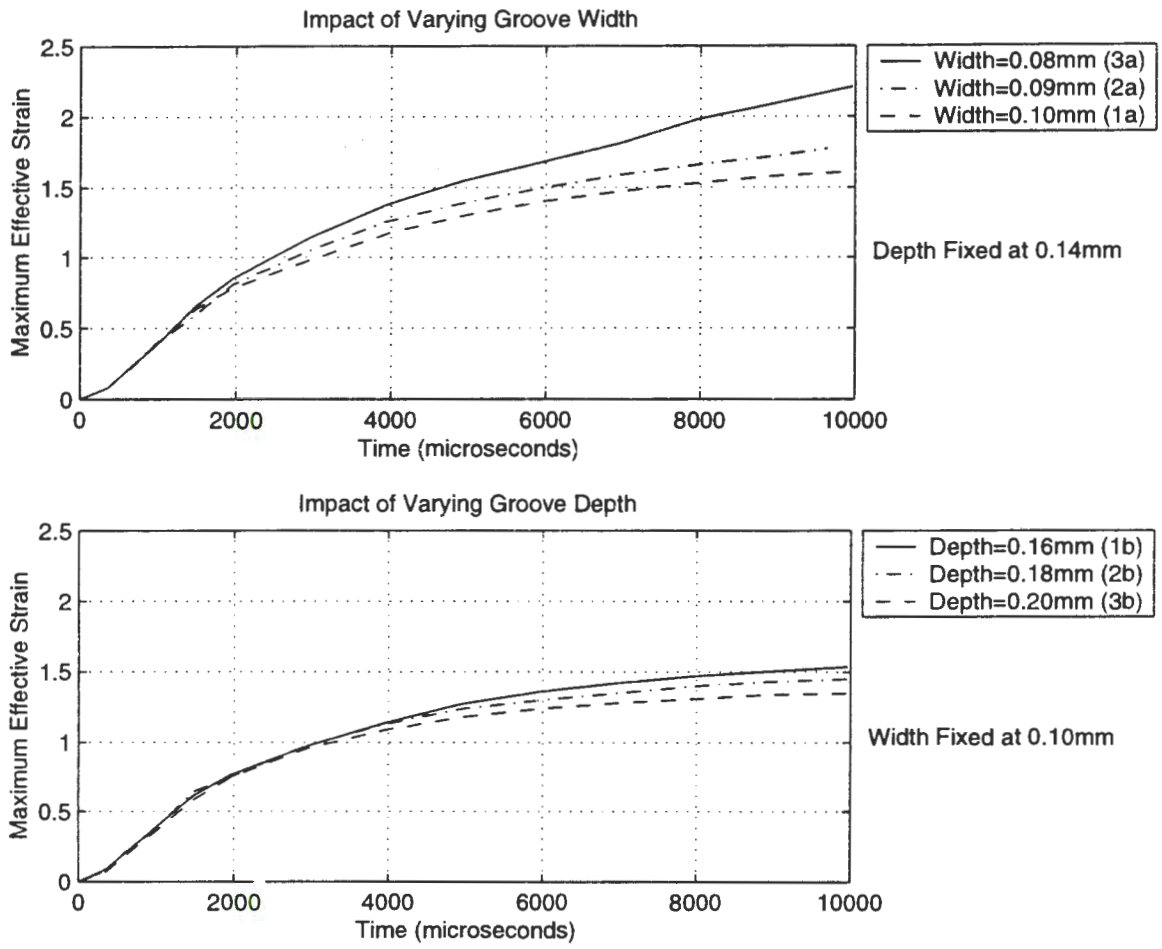

Figure 2.10 Effective strain in the free surface of the chip root

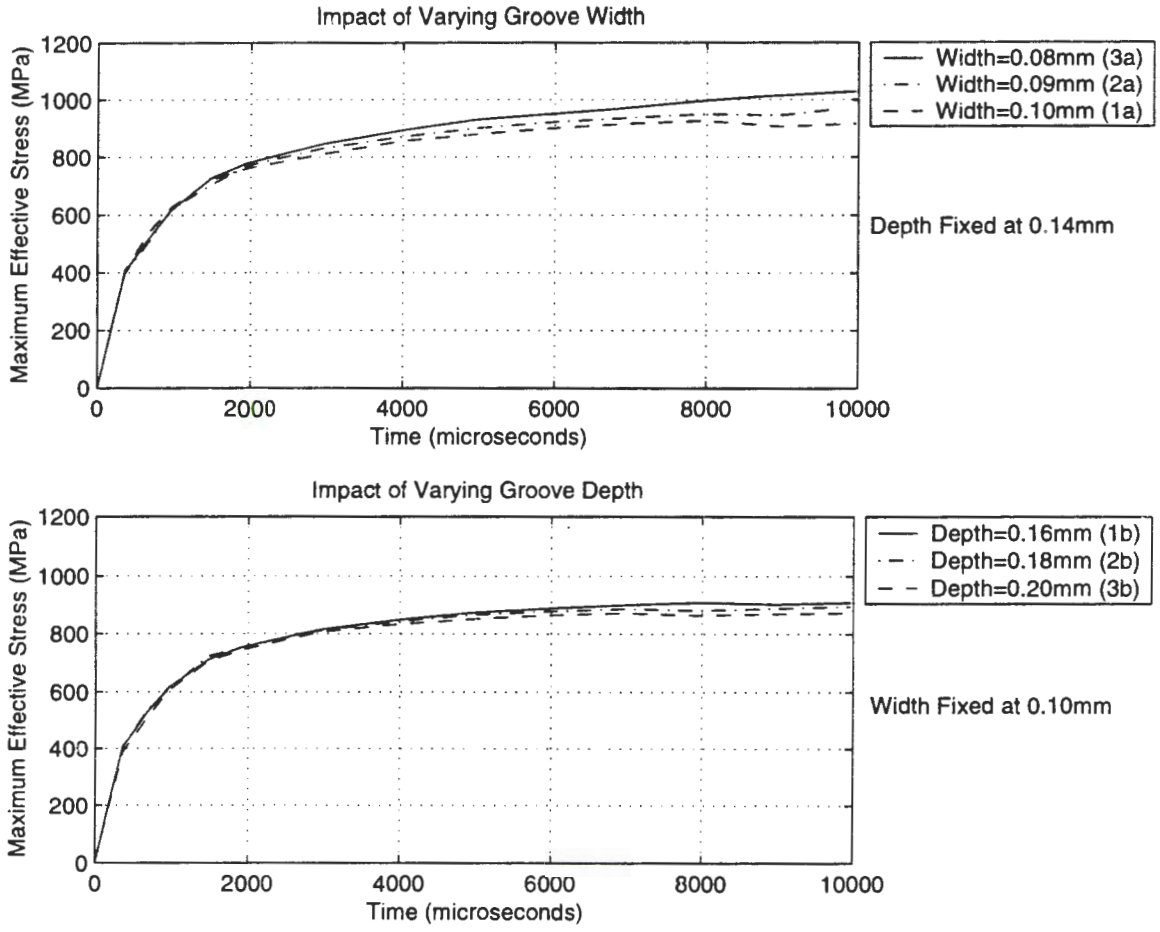

Figure 2.11 Effective stress in the free surface of the chip root

3 VALIDATION OF A FINITE ELEMENT ORTHOGONAL CUTTING MODEL

A paper to be submitted to the Journal of Material Processing Technology

B. McClain, S. Batzer, and G.I. Maldonado

Abstract

This paper presents the development of an orthogonal cutting model using DYNA3D finite element analysis software. The Johnson-Cook constitutive model [1] for O1 tool steel was incorporated into the simulation in order to account for the effects of strain hardening, strain rate hardening and thermal softening. The model was then compared to experimentally measured cutting forces in order to verify its accuracy. The model successfully predicted the cutting forces, stress distribution at the tool-chip interface, and the effects of specific heat and friction on cutting forces and chip geometry.

3.1 Introduction

The study of chip formation in metal cutting has proven to be a complex undertaking, and much work is left to be done before an entirely accurate machining model is developed. Early machining models were analytical in nature and based on experimental observations. The complex nature of the machining process has made the development of accurate analytical models difficult, and numerical models have become popular. Advances in finite element theory, coupled with rapidly developing computer technology, have led to increasing use of finite element analysis in machining models since the 1970's.

Two different viewpoints, Lagrangian and Eulerian, may be employed to describe a continuous medium with a finite element model [2]. The Eulerian finite element formulation, typically used to study the motion of fluids, focuses on a fixed point in space and examines changes in the matter passing through that point. This method requires only a small number of elements, and therefore is computationally efficient. In addition, it is unnecessary to predefine the line along which the chip

separates from the workpiece. However, the Eulerian method is only capable of simulating steady state cutting conditions. This method has been successfully employed in metal cutting simulations by researchers such as Strenkowski [3, 4].

Most metal cutting simulations have employed the Lagrangian formulation [5-12]. This method focuses on a fixed set of material particles and follows them regardless of their location. The Lagrangian formulation is capable of simulating chip formation from the incipient stages to steady state cutting. However, it is computationally intensive due to the larger number of elements required. In addition, it is necessary to predefine a parting line for the chip and determine an appropriate element separation criterion.

Element separation criteria may be based on physical properties, such as the shear and normal failure stresses of the workpiece, or on geometric considerations like the distance between the tool tip and the edge of the element. Several researchers have studied the effects of different element separation criteria in orthogonal cutting simulations. Black and Huang recommended that a combination of physical and geometric criteria be used in cutting simulations [13]. It was suggested by Zhang and Bagchi the geometric criterion should be between 10 and 30 percent of the workpiece elemental length for best results [14].

3.2 Finite Element Model

The orthogonal cutting simulations in this paper were created using a modified version of the research-licensed FEM code DYNA3D [15]. DYNA3D is an explicit, nonlinear, finite element code which uses the updated Lagrangian formulation to model complex material behavior in three-dimensional structures. Symmetry planes were used to constrain the element deformations to two dimensions in order to simulate orthogonal cutting conditions. A representative finite element model illustrating the undeformed mesh is shown in Figure 3.2. The tool and workpiece were both modeled with eight-node brick elements. Since the tool was considered to be perfectly sharp and rigid, it was modeled with a much coarser mesh. The workpiece was modeled with the same number of elements in each simulation, so the height of the elements varies slightly for different cutting depths.

To simulate cutting, the bottom of the workpiece was fixed in the x and y directions, and the tool was defined to have a constant velocity in the negative x direction. The chip was defined to separate from the workpiece along the line A-B. Two types of slide surfaces available in DYNA3D were used to model the chip separation and friction between surfaces in contact. Regions 1 and 2 of the workpiece were joined with a *tied with failure* slide surface [15]. This type of slide surface joins two surfaces until

a failure criterion is met. In DYNA3D, failure occurs when the following condition is met:

$$\left(\frac{F_n}{F_{nf}}\right)^2 + \left(\frac{F_s}{F_{sf}}\right)^2 \geq 1 \tag{3.1}$$

where F_n and F_s are the total normal and shear forces acting on the segment, and F_{nf} and F_{ns} are the normal and shear failure forces of the segment. The normal and shear forces are computed internally during the simulation, and the normal and shear failure stresses are specified by the user beforehand. In addition to this physical criterion, a geometric separation criterion was added to the source code by Thean [16]. The nodes connecting Region 1 and Region 2 will separate either when Equation 3.1 is satisfied or when the distance between the tip of the tool and that particular node is less than a specified distance criterion. The distance criterion was set equal to 10 percent of the length of the workpiece elements. In a study performed by Zhang and Bagchi [14], the use of a 10 percent distance criterion was found to minimize the crack between the tool and chip without causing numerical instability.

Once the elements have separated, contact between the chip and tool is modeled by a *sliding with separation and friction* slide surface [15]. This slide surfaces allows the elements to slide freely and come into contact or separate from each other at any time. A penalty function is used to limit penetration of the surfaces to a degree specified by the user. Friction between the two surfaces is modeled as Coulombic, and for the initial simulations in this study, a constant coefficient of friction was used with $\mu = 0.1$. A value of 0.1 was chosen for the initial simulations because higher values were found to cause numerical instabilities in the program.

The mechanical behavior of the workpiece was modeled with the Johnson-Cook constitutive model [1] using the properties of O1 tool steel. This model accounts for the effects of strain, strain rate, and temperature rise, which are significant factors in machining of steel. In the Johnson-Cook model, the stress-strain curve is given by the following equation:

$$\sigma = [A + B(\bar{\epsilon}^p)^n][1 + Cln(\frac{\bar{\epsilon}^p}{\dot{\epsilon}_0})][1 - (\frac{T - T_r}{T_m - T_r})^m] \tag{3.2}$$

where $\bar{\epsilon}^p$ is the effective plastic strain, $\dot{\epsilon}_0$ is the reference strain rate, T is the temperature in the material, T_m is the melting temperature of the material, T_r is the room temperature, and A, B, C, n, and m are material dependent constants. Heat is generated in the elements as a result of plastic work. The Johnson-Cook constitutive model constants for O1 tool steel were experimentally determined by Batzer [17], and the density, specific heat, and shear modulus were based on typical values for steel. Table 3.1 lists the material properties used for the simulations in this paper.

Table 3.1 Material properties for O1 tool steel

ρ (Kg/m^3)	c_p (J/KgK)	G (MPa)	T_m (K)	A (MPa)	B (MPa)	$\dot{\epsilon_o}$ (s^-1)	n -	C -	m -
7801	477	83	1728	391.3	723.9	65.3	0.3067	0.1144	0.9276

3.3 Comparison with Experimental Results

Results from the finite element model were compared to experimentally measured results in order to gauge the accuracy of the simulation. A total of eight tests were simulated, using two rake angles, cutting speeds, and feeds. The parameters used in each simulation are summarized in Table 3.2. The results of these simulations were then compared to orthogonal cutting tests performed by Batzer [17]. The cutting tests were performed using a disk of O1 steel approximately 4 mm wide and a flat faced cutting tool. A Cincinnati Milacron Cinturn 8C Series 1208 CNC lathe was used to machine the disks at a constant surface speed, and a strain gauge dynamometer was used to measure the cutting and thrust forces.

Figure 3.1 displays the contours of effective stress and strain simulated in Case 4. Although the magnitude of the contours varied, the contours were similarly shaped for all cases. The highest stress values were found in the shear plane, while the highest strains occurred on the outside edge of the chip. The increased strain on the outside edge of the chip is due in part to the deformation which occurs along the rake face as a result of frictional forces between the tool and chip.

Table 3.3 presents a comparison between the experimentally measured forces and simulated results. Although the cutting forces, F_c, show good agreement in most cases, examination of the table exposes several deficiencies in the model. The simulated cutting forces are all within 16% of the experimental measurements, but the thrust forces differ by as much as 97%. This can be explained in part by the low value used for the coefficient of friction in this test, $\mu = 0.1$. Since the coefficient of friction may be defined as the ratio of the forces acting parallel and perpendicular to the sliding plane, the ratio between the thrust force and the cutting force will be equal to the coefficient of friction for the zero degree rake angle cases. As a result, the magnitude of the simulated thrust force was found to be one tenth the magnitude of the cutting force for the simulations with zero degree rake angles. This indicates that a value of 0.1 is inadequate for the coefficient of friction. A comparison of the experimentally measured forces indicates that the cutting conditions would be more accurately represented by a coefficient of friction between 0.4 and 0.5.

Examination of the forces measured at different speeds indicates another inaccuracy in the model.

Table 3.2 Parameters for flat faced tool simulation

Simulation	Rake Angle	Width of Cut	Depth of Cut	Cutting Speed
1	0	4.013 mm (0.158 in)	0.01016 cm (0.004 in)	279.4 cm/s (550 sfm)
2	0	4.013 mm (0.158 in)	0.01016 cm (0.004 in)	406.4 cm/s (800 sfm)
3	0	4.013 mm (0.158 in)	0.01524 cm (0.006 in)	279.4 cm/s (550 sfm)
4	0	4.013 mm (0.158 in)	0.01524 cm (0.006 in)	406.4 cm/s (800 sfm)
5	5	3.861 mm (0.152 in)	0.01016 cm (0.004 in)	279.4 cm/s (550 sfm)
6	5	3.861 mm (0.152 in)	0.01016 cm (0.004 in)	406.4 cm/s (800 sfm)
7	5	3.861 mm (0.152 in)	0.01524 cm (0.006 in)	279.4 cm/s (550 sfm)
8	5	3.861 mm (0.152 in)	0.01524 cm (0.006 in)	406.4 cm/s (800 sfm)

Table 3.3 Results of flat faced tool simulation

Simulation	Experimental F_c (lbf)	Simulated F_c (lbf)	Error (%)	Experimental F_t (lbf)	Simulated F_t (lbf)	Error (%)
1	225.4	195.7	13.2	114.4	19.5	83.0
2	216.8	198.2	8.6	103.5	19.7	81.0
3	330.4	286.3	13.3	154.1	28.6	81.4
4	298.1	290.7	2.5	113.5	29.0	74.4
5	205.3	173.1	15.7	75.6	2.1	97.2
6	184.0	176.0	4.3	65.0	2.1	96.8
7	289.4	252.7	12.7	99.7	3.1	96.7
8	270.7	257.9	4.7	81.6	3.2	96.1

The simulated forces for the higher cutting speed are consistently higher than forces simulated at the lower cutting speed, while the experimental results showed the forces actually decreased with increasing cutting speed. As a result, the error between simulated and measured forces is significantly higher for all cases at the slower speed.

In order to further investigate the effect of cutting speed on the simulated results, four additional simulations were compared. In all four simulations, the conditions were identical to those used in Case 4. Only the cutting speed was varied. Table 3.4 shows the effect of varying the cutting speed from 100 sfm to 1500 sfm on the simulated results. The cutting forces are observed to increase with increasing cutting speed while the measured shear plane angle, ϕ, is virtually unchanged. This is inconsistent with experimental observations which show that as the cutting speed increases, ϕ increases and the cutting forces decrease [18].

An additional study was conducted to examine the effect of the coefficient of friction on the model. In this study, Case 4 was repeated with values of μ varying from 0.0 to 0.2. As can be seen in Table 3.5, increasing the coefficient of friction leads to decreased shear plane angles and increased cutting forces.

Table 3.4 Effect of cutting speed

Cutting speed sfm	Cutting Force (F_c) lbf	Shear plane angle (ϕ) degrees
100	263	31
550	286	34
800	291	34
1500	298	34

These are the expected trends. In addition, the value chosen for the coefficient of friction was found to have a significant impact on the resulting shape of the chip. Figure 3.3 shows the resulting chip at the same point in time for simulations using three different values for μ. The figure clearly shows that using higher values of μ in the simulations produces chips with less curl than in the simulations using low coefficients of friction. It is believed that the chip shown in Figure 3.3c more accurately represents the chip's curvature.

Table 3.5 Effect of friction

μ	Cutting Force (F_c) lbf	Shear plane angle (ϕ) degrees
0.0	267	37
0.05	277	35
0.1	291	34
0.2	312	32

Despite the deficiencies in the model, the stress distribution on the rake face was accurately predicted. Figure 3.4 represents the stress distribution at the rake face simulated in Case 4. The simulation produced shear and normal stress distributions that plateaued near the tool tip and then dropped near the end of the tool-chip contact region. The normal stress was found to be much higher than the shear stress until approaching the end of the tool-chip contact region. These stress distributions closely resemble the shape and relative magnitudes of experimental measurements performed by Buryta using a split tool dynamometer [19].

3.4 Discussion

The error found in the initial simulations may be attributed to three main factors. First, considering the coefficient of friction to remain constant at a value of 0.1 is not adequate for modeling most machining conditions. Observation of the experimentally measured forces indicated that the average value of μ

should be between 0.4 and 0.5 for the conditions studied in this paper. In addition, it has been shown that the coefficient of friction does not remain constant along the tool-chip interface. There is actually a region of sticking friction near the tool tip and a region of sliding friction away from the cutting edge [18], as shown in Figure 3.5. In the sticking region, the chip is deformed in shear by high frictional stresses. This region corresponds to the region of the high plateau of shear and normal stress in Figure 3.4. In the sliding region, the frictional stresses are much lower, and the shear deformation does not occur as in the sticking region. Most researchers agree that the sticking region and sliding region are roughly equal in length.

Second, the Johnson/Cook material model in DYNA3D assumes adiabatic conditions. As a result, there is no heat conducted between the elements. Heat conduction is an important factor in machining, having a significant influence on the shear plane angle. During the cutting process, heat is generated in the shear plane as a result of the work done in deforming the chip. Some of this heat is lost with the chip, and a portion of it is conducted back into the workpiece, softening the material. This will increase the shear plane angle and decrease the chip thickness and cutting forces. Due to the limitations of the software, it is not possible to directly model this phenomenon. That is, the conductivity of the material is implicitly zero. Since the amount of heat conducted back into the workpiece will be affected by the cutting speed, this could partially explain the incorrect trend of increasing cutting forces resulting from increasing cutting speeds obtained in the simulations.

Finally, an average value was used for the specific heat in all simulations because the Johnson/Cook constitutive model in DYNA3D does not have the capability to vary the specific heat during the simulation. In reality, the specific heat varies as a function of temperature. As the workpiece temperature increases, the specific heat should increase as well. As the specific heat increases, more energy is required to raise the temperature of the workpiece. As a result, the amount of heat generated and the rate of thermal softening will be decreased as the temperature rises. Since the specific heat is a function of temperature, and the rate of heat generation in the workpiece is related to the cutting speed, the constant value used for the specific heat in the simulations will also impact the relationship of the simulated cutting forces to the cutting speed.

The effect of specific heat on the cutting forces is illustrated in Figure 3.6. In this test, Case 4 was repeated with three different values of c_p. The specific heat was 477 J/KgK in the first simulation, the same value used in the previous tests. Simulations were run with a lowered value of c_p, 300 J/KgK, and with an arbitrarily high value, $1 * 10^{10}$ J/KgK. Decreasing the specific heat of the material was found to decrease the cutting force as expected. When c_p was made arbitrarily high, the thermal softening

effect was eliminated and the cutting forces were dramatically increased. In this case, steady state had not been reached after 300 microseconds because the chip thickness was still increasing. Figure 3.7 illustrates the effect of specific heat on the chip shape. As the specific heat increases, the chip thickness increases and the shear plane angle and degree of chip curl decreases.

Due to the inability of DYNA3D to model heat conduction into the workpiece and the variation of specific heat with temperature, the rate of thermal softening in the workpiece will be unaffected by the cutting speed. The only velocity dependent term remaining in the constitutive model will therefore be the strain rate. Since the strain rate increases with increasing cutting speed, the strain rate hardening effect will also increase. As a result of the increasing rate hardening effect, which is not balanced by a velocity-dependent thermal effect, the simulated cutting forces will increase as the cutting speed increases.

Although the model is limited by the capabilities of DYNA3D, it is accurate in many respects. The predicted cutting forces were within 16% of the experimentally measured values for all cases studied. This is good agreement for a numerical model of such a complex process. In addition, the predicted shear and normal stress distributions at the tool-chip interface accurately reproduce experimentally measured distributions in the literature [19]. Finally, variations in μ and c_p in the simulations affected the cutting forces and chip geometry as expected. This indicates that the model is useful, needing only some fine tuning.

3.5 Future Work

3.5.1 Improved Friction Model

As was mentioned previously, assuming a constant coefficient of friction on the rake face does not adequately represent the complex interaction between the chip and the tool. Future models will include a sticking zone and a sliding region. The first half of the tool-chip contact length, nearest the tool tip, will be considered to be the sticking region. This zone will have an increased value for the coefficient of friction, $\mu = 0.7$. The second half of the tool-chip contact length will represent the sliding region. In this zone, the coefficient of friction will remain 0.1 as before. Since the tool-chip contact length varies with cutting speed, it will be necessary to adjust the length of the sticking and sliding regions for each speed simulated. In this way, a more accurate representation of the tool chip interaction is obtained.

3.5.2 Determination of Specific Heat

Since the Johnson/Cook constitutive model in DYNA3D does not account for the effects of heat conduction or the dependence of specific heat on temperature, it is necessary to incorporate a method to account for the variation in the degree of thermal softening at different cutting speeds. The key factor determining the degree of thermal softening in the model is the value chosen for the specific heat. Therefore, the varying degrees of thermal softening may be accounted for by choosing a different value for c_p for each cutting velocity simulated. The appropriate value for the specific heat will be determined using an iterative procedure.

The first step in determining the appropriate value for c_p will be to run a simulation using the desired rake angle (α), cutting width (b), cutting speed (V), and feed (t_0). The simulation will return values for the cutting force (F_c) and the shear plane angle (Φ). The shear plane angle may then be used to calculate the shear strain (γ) in the material as follows:

$$\gamma = \frac{\cos(\alpha)}{\sin(\Phi)\cos(\Phi - \alpha)} \tag{3.3}$$

The specific shear energy (u_s) may also be calculated using the following equation:

$$u_s = \frac{F_c}{bt_0} \tag{3.4}$$

Next, the temperature in the shear plane may be estimated using the model developed by Lowen and Shaw [20]. This model assumes that the temperature rise in the shear plane is equivalent to the amount of energy carried away by the chip, and therefore, the temperature in the shear plane may be calculated as follows:

$$T = T_0 + \frac{R_1 u_s}{JC_1\rho_1} \tag{3.5}$$

where T is the resulting temperature in the shear plane and T_o is the initial temperature. J is the mechanical equivalent of work, which is equal to 1 when SI units are used, and ρ is the density of the workpiece which is assumed to remain constant. C_1 is the volumetric specific heat (also denoted c_v), which varies as a function of temperature. R_1 is the fraction of the energy which is carried away by the chip, and therefore (1-R_1) is the fraction of the energy conducted into the workpiece. The value of R_1 is calculated via the following equation:

$$R = \frac{1}{1 + 1.328\left[\frac{K_1\gamma}{Vt_0}\right]} \tag{3.6}$$

where V is the cutting speed and t_0 is the undeformed chip thickness, both initial inputs to the simulation. K_1 is the diffusivity of the workpiece given by the following equation:

$$K_1 = \frac{k_1}{\rho c_p} \tag{3.7}$$

where k_1 is the conductivity of the workpiece, a known constant. Since both c_p and c_v are themselves functions of temperature, Equations 3.5, 3.6, and 3.7 must be solved numerically through an iterative process to obtain an estimate for the temperature on the shear plane.

Once the shear plane temperature is calculated, it may be compared with the shear plane temperature calculated by DYNA3D (T_{Dyna}). DYNA3D calculates the temperature rise assuming a constant specific heat based on the amount of plastic work done as follows:

$$T_{Dyna} = T_0 + \frac{\int \sigma d\epsilon}{c_v} \tag{3.8}$$

which may be written in terms of known values:

$$T_{Dyna} = T_0 + \frac{\frac{F_c}{bt_0}}{c_v} \tag{3.9}$$

The final step in the process is to compare the values of T and T_{Dyna}. The value used in the simulation for the specific heat will be decreased if T_{Dyna} is less than T and increased if T_{Dyna} is greater than T. The simulation will then be rerun with the new c_p and the temperatures will be compared again. This process will be repeated until reasonable agreement is reached. The final value of c_p will be used in all simulations performed at the same cutting speed. The specific heat will be recalculated in the same manner for each cutting speed to be used in the simulations.

3.6 Conclusion

The simulations developed for this paper were able to predict experimentally measured cutting forces with less than 16 percent error, a reasonable margin for such simulations. The simulations were also able to accurately predict the stress distribution at the tool-chip interface. In addition, test cases performed as expected when the specific heat and coefficient of friction were varied in the model. The errors evident in the model can be attributed to three major factors, namely the constant value used for the coefficient of friction in this study, and the inability of DYNA3D to model heat conduction and variations in the specific heat with changes in temperature. These concerns will be addressed in future work.

Bibliography

[1] Johnson, G.R., Cook, W.H., 1983, "A Constitutive Model and Data for Metals Subjected to Large Strains, High Strain Rates, and High Temperatures," *Proceedings of the Seventh International Symposium on Ballistics*, the Hague, The Netherlands.

[2] Reddy, J.N., 1993, *An Introduction to the Finite Element Method*, McGraw-Hill, Inc.

[3] Strenkowski, J.S., Carroll, J.T., 1986, "An Orthogonal Metal Cutting Model Based on an Eulerian Finite Element Method," *Manufacturing Processes, Machines and Systems*, Proceedings of the 13th Conference on Production Research and Technology, Society of Manufacturing Engineers, Dearborn, MI, pp. 262-264.

[4] Strenkowski, J.S., Moon, K., 1990, "Finite Element Prediction of Chip Geometry and Tool/Workpiece Temperature Distributions in Orthogonal Metal Cutting," *Journal of Engineering for Industry*, Vol. 112, pp. 313-318.

[5] Shih, A.J.M., Chandrasekar, S., Yang, H.T.Y., 1990, "Finite Element Simulation of Metal Cutting Process with Strain-Rate and Temperature Effects," *Fundamental Issues in Machining*, ASME Publication PED — Vol. 43, New York, N.Y., pp. 11-24.

[6] Shih. A.J., 1995, "Finite Element Simulation of Orthogonal Metal Cutting," *ASME Journal of Engineering for Industry*, Vol. 117, pp. 84-93.

[7] Shih, A.J., 1996, "Finite Element Analysis of The Rake Angle Effects in Orthogonal Metal Cutting," *Int. Jour. Mech. Sci.*, Vol. 38, pp. 1-17.

[8] Komvopoulos, K., Erpenbeck, S.A., 1991, "Finite Element Modeling of Orthogonal Metal Cutting," *ASME Journal of Engineering for Industry*, Vol. 113, pp. 253-267.

[9] Zhang, B., Bagchi, A., 1994, "Finite Element Simulation of Chip Formation and Comparison with Machining Experiment," *ASME Journal of Engineering for Industry*, Vol. 116, pp. 289-297.

[10] Lin, Z.C., Pan, W.C., Lo, S.P., 1995, "A Study of Orthogonal Cutting with Tool Flank Wear and Sticking Behavior on the Chip-Tool Interface," *Journal of Materials Processing Technology*, Vol. 52, pp. 524-538.

[11] Eldridge, K.F., Dillon, O.W., Lu, W., 1991, "Thermo-Viscoplastic Finite Element Modeling of Machining Under Various Cutting Conditions," *Transactions of NAMRI/SME*, pp. 162-169.

[12] Kim, K.W., Sin, H., 1995, "Development of a Thermo-Viscoplastic Cutting Model Using Finite Element Method," *International Journal of Machine Tools Manufacturing*, Vol. 36, No. 3, pp. 379-397.

[13] Huang, J.M., Black, J.T., 1996, "An Evaluation of Chip Separation Criteria for the FEM Simulation of Machining," *Journal of Manufacturing Science and Engineering*, Vol. 118, pp. 545-554.

[14] Zhang, B., Bagchi, A., 1994, "A Study of Chip Separation and Its Approximation in Finite element Simulation of Continuous chip Formation," *The Physics of Machining Processes - II* , ASME Minerals, Metals & Materials Soc., p. 157.

[15] Whirley, R.G., Engelmann, B.E., 1993, "DYNA3D: A Nonlinear, Explicit, Three-Dimensional Finite Element Code For Solid and Structural Mechanics – User Manual," *Lawrence Livermore National Laboratory Report UCRL-MA-10752.*

[16] Thean, W.K., McClain, B., Maldonado, G.I., Fang, X.D., 1999, "Finite Element Analysis of Chip Formation in Grooved Tool Metal Cutting," under review by the *Journal of Machining Sciences and Technology.*

[17] Batzer, S.A., 1998, *An Analytical and Experimental Investigation into Chip Morphology in Orthogonal Machining,* PhD Thesis, Michigan Technological University.

[18] Stephenson, D.A., Agapiou, J.S., 1997, *Metal Cutting Theory and Practice*, Marcel Dekker Inc., New York.

[19] Buryta, D., Sowerby, R., Yellowley, I., 1994, "Stress Distributions on the Rake Face During Orthogonal Machining," *International Journal of Machine Tools Manufacturing*, Vol. 34, No. 5, pp. 721-739.

[20] Lowen, E.G., Shaw, M.C., 1954, "On the Analysis of Cutting-Tool Temperatures," *ASME Journal of Engineering for Industry*, Vol. 76, pp. 217-231.

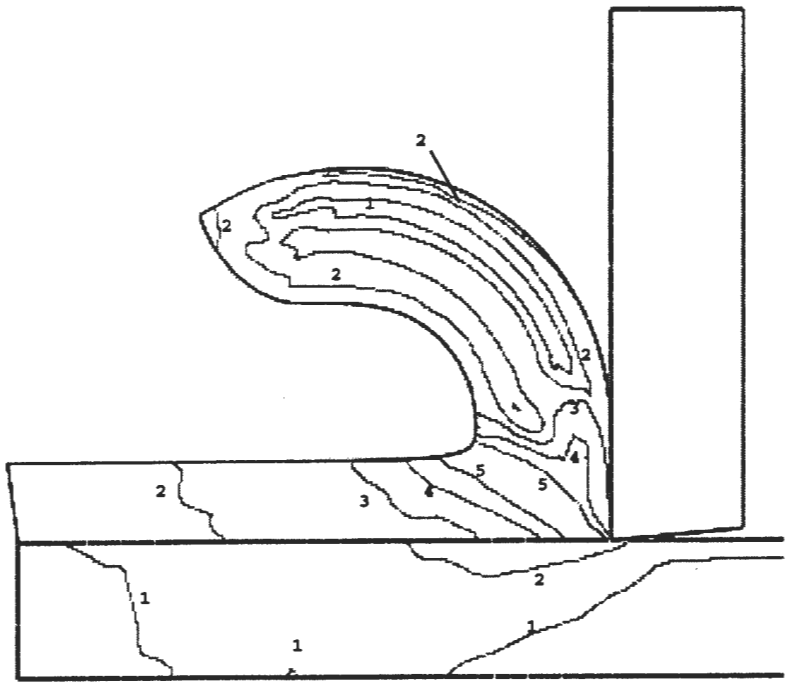

(a)

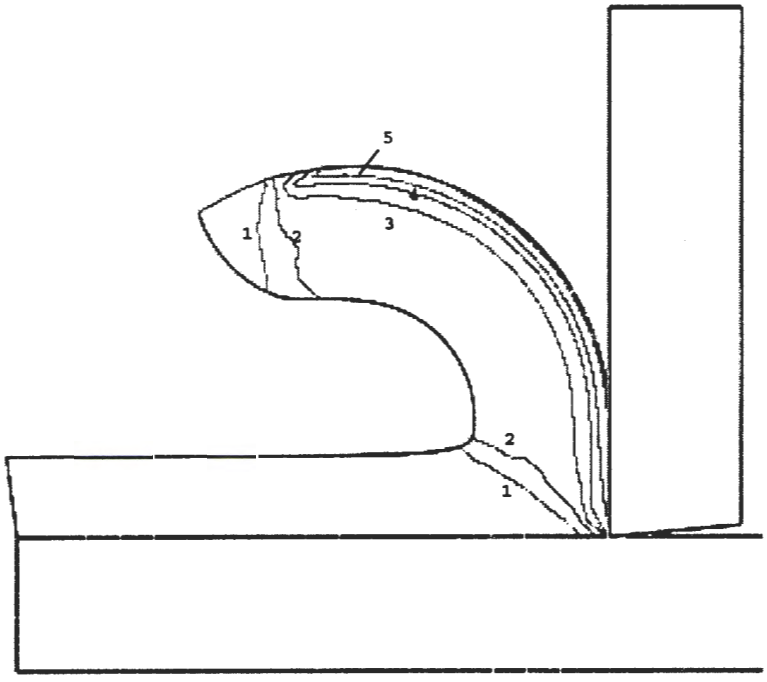

(b)

Figure 3.1 Case 4: (a) Effective stress (b) Effective strain

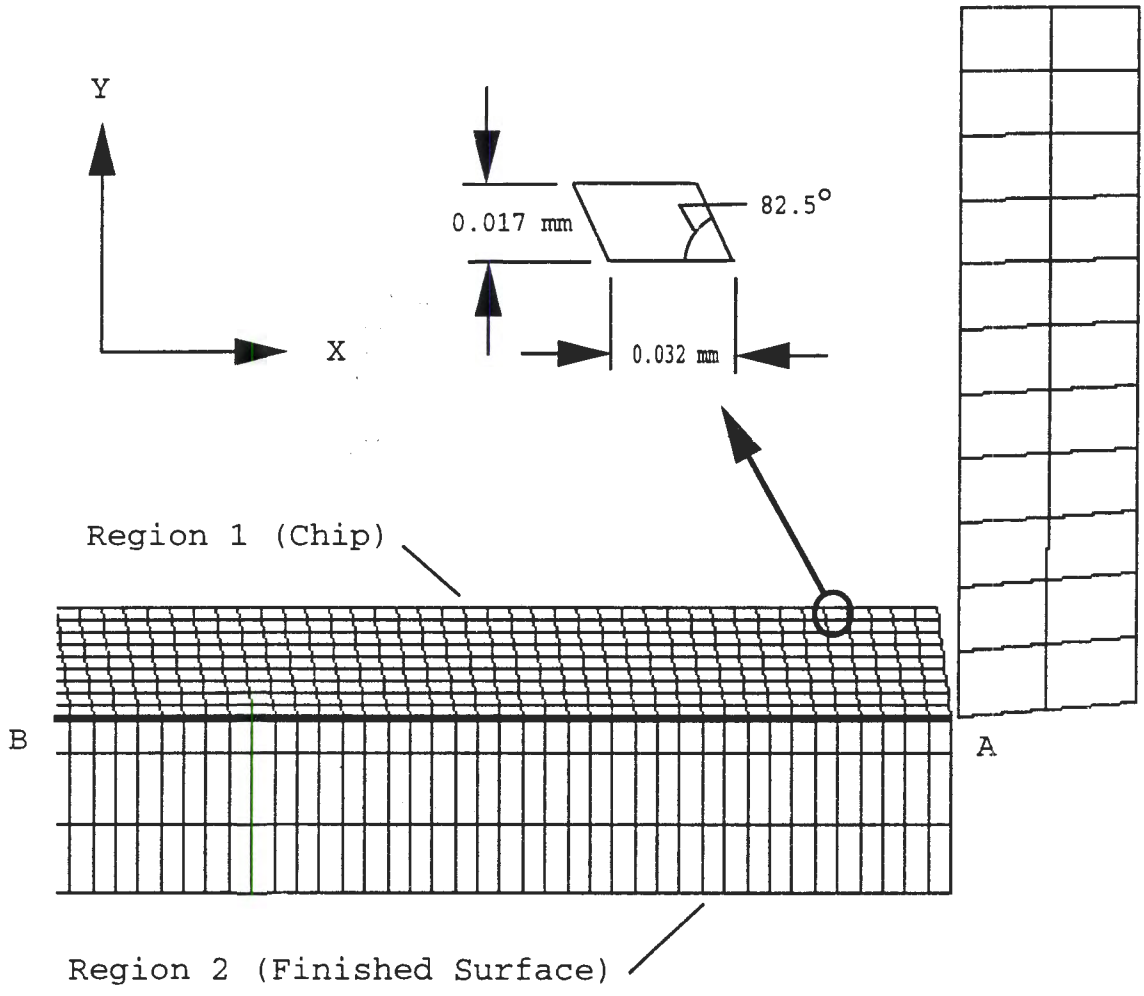

Figure 3.2 Representative undeformed finite element model

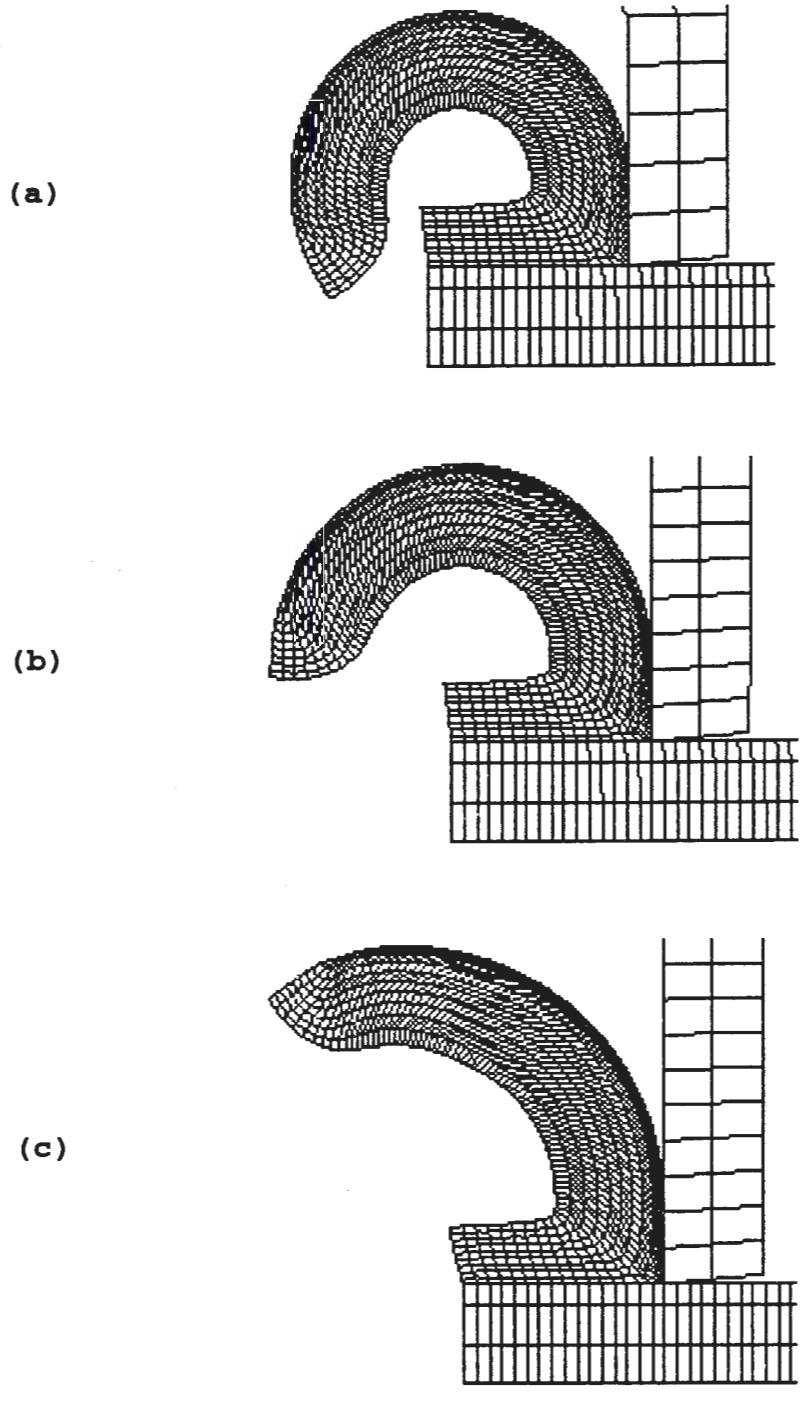

Figure 3.3 Effect of friction on chip curl: (a) $\mu = 0.05$ (b) $\mu = 0.1$ (c) $\mu = 0.2$

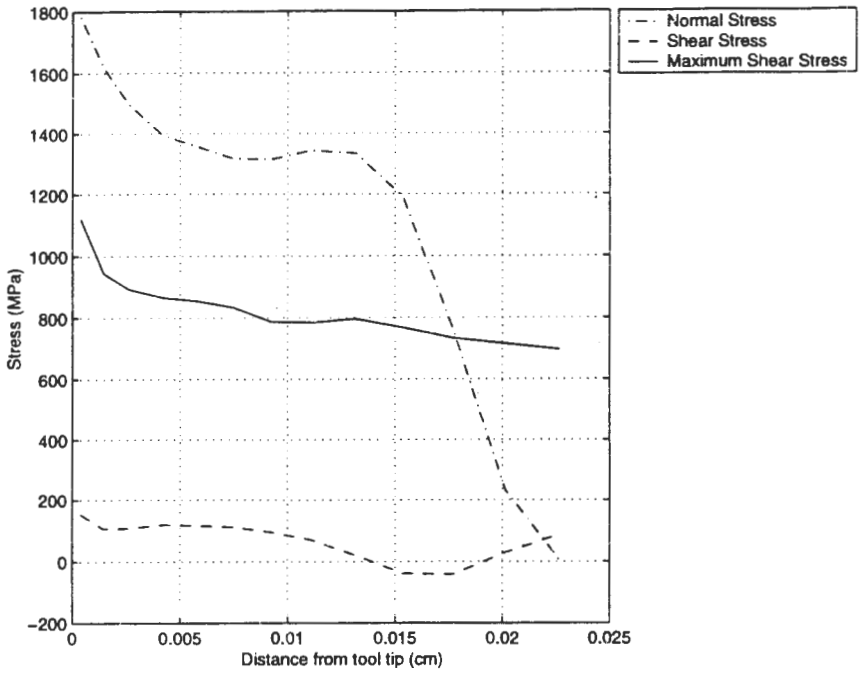

Figure 3.4 Stress distribution on the rake face for Case 4

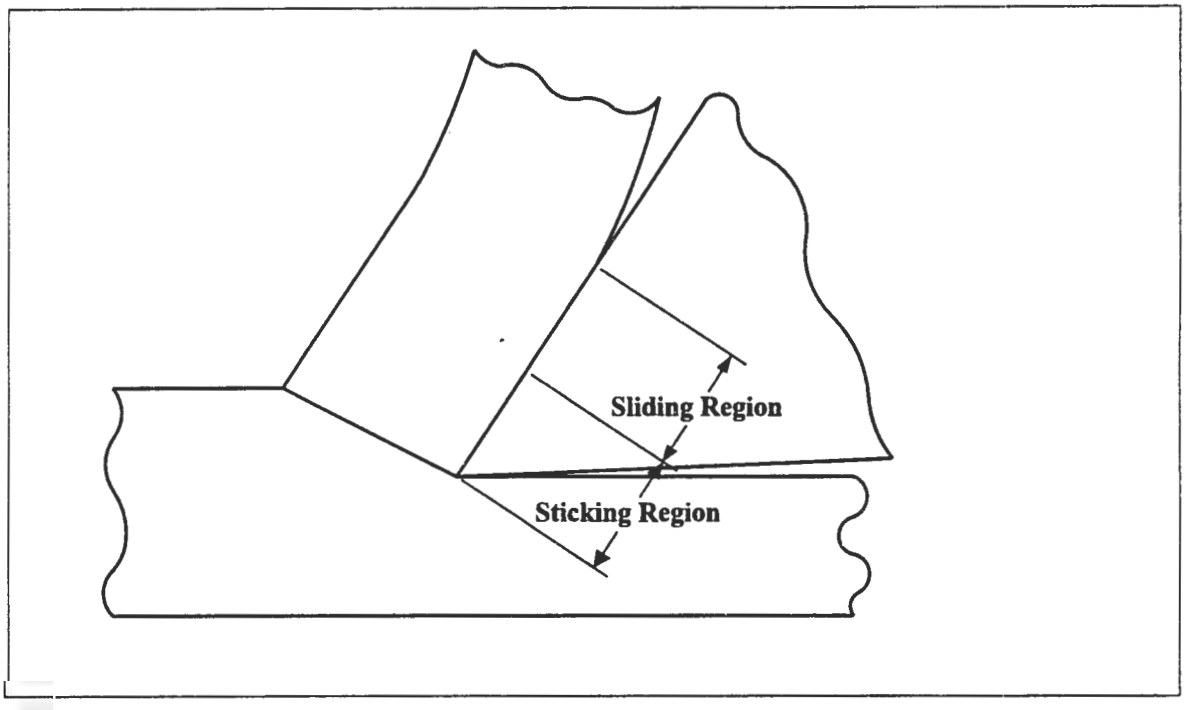

Figure 3.5 Friction zones at tool-chip interface

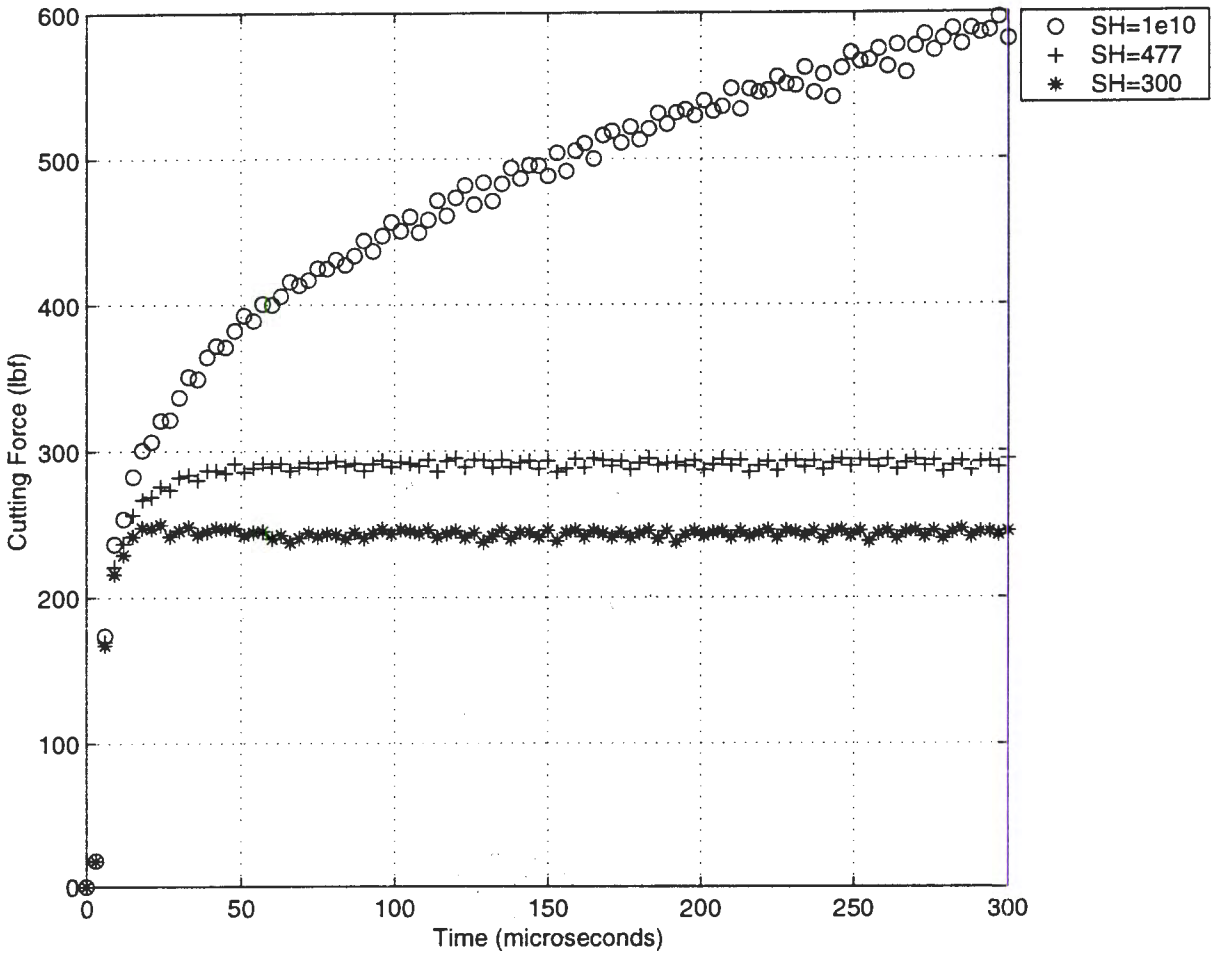

Figure 3.6 Effects of specific heat on cutting forces

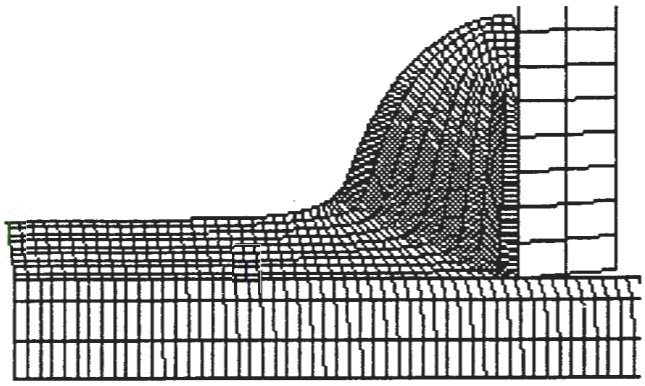

(a)

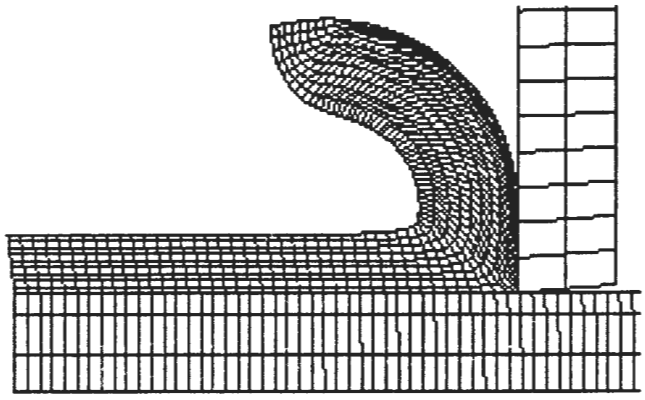

(b)

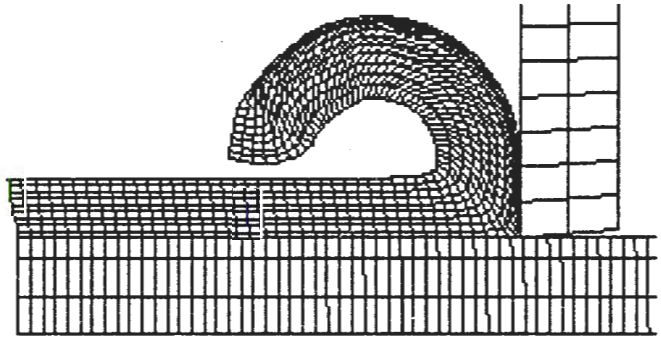

(c)

Figure 3.7 Effect of specific heat on chip geometry: (a) $c_p = 1e10 J/KgK$ (b) $c_p = 477 J/KgK$ (c) $c_p = 300 J/KgK$

4 CONCLUSION

4.1 Discussion of Results

The simulations presented in this thesis represent two stages in the development of an accurate finite element machining model. In the first paper, a simple machining model was developed. This model was limited in the respect that it used a power law strain hardening constitutive model to represent the mechanical behavior of the workpiece material. Such a model does not account for the effects of strain rate hardening or thermal softening, both significant factors in machining. Despite the use of a simplified material model, it is believed that these simulations are of value. The intent of the first paper was to study the effect of varying groove geometry on chip formation. Although the use of a simplified material model will affect the magnitudes of the stress and strain contours calculated for the chip, the conclusions should still be valid since they focus on general trends resulting from the changes in groove geometry.

In the second paper, a much more sophisticated machining model was developed. The simulations developed in the paper incorporate a Johnson/Cook constitutive model which takes into account the effects of strain rate hardening and thermal softening. The improved model was shown to be capable of accurately simulating experimentally measured results. In particular, the model closely predicted experimentally measured cutting forces and exhibited stress distributions at the tool-chip interface which were in agreement with published results. In addition, the effects of varying the specific heat and coefficient of friction between the chip and tool were both accurately predicted by the model. Although the second model is greatly improved, the results are in error in some respects. The simulated thrust forces were much lower than the expected values. In addition, the simulated cutting forces were found to increase as the cutting speed increased. In reality, the cutting forces should decrease. These errors can be attributed to two main factors. First, the coefficient of friction employed in the simulations was too low to realistically represent the tool-chip interaction. Second, the Johnson/Cook constitutive model used by DYNA3D does not have the capability to model heat conduction or the variation of specific heat with temperature. Although the current simulations provide valuable information, these

issues must be resolved by future researchers in order for the simulations to be completely accurate.

4.2 Future work

Development of an accurate machining model is a complex undertaking, and many areas remain for future researchers to investigate. The first issue that should be addressed is the method used to model the friction between the tool and chip. The simulations in this work used a constant coefficient of friction with a value of 0.1. This value is too low to accurately model most machining operations and does not account for the presence of the sticking and sliding friction regions. Future models should include a region of higher friction near the tool tip, the sticking region, and a region of lower friction away from the tool tip, the sliding region.

Another concern which should be addressed is the effect of thermal softening. DYNA3D does not account for heat conduction or variations in the value of specific heat. As a result, it will be necessary to determine a representative value for the specific heat for each new cutting speed that is simulated. This may be done through an iterative process as discussed in the second paper. A study by the author will address these issues, and additional orthogonal machining experiments will be performed in order to provide validation for the new methods. The results of this study will be submitted for publication in the future.

In addition to the studies to be performed by the author, many fertile areas remain for future researchers to explore. Although it would be difficult, it would be possible to modify the DYNA3D source code to include a heat conduction subroutine and a specific heat function that varies with temperature. This would require considerable programming expertise, but it would make the simulations more user friendly. This would eliminate the need to iteratively determine the specific heat for each cutting speed, resulting in a more predictive model.

The simulations in this paper modeled the tool as rigid and perfectly sharp. Although these are common assumptions in machining models, they are not completely true to life. In reality the tool is not rigid, and tool wear will occur over time during machining. In actuality, the tool is not perfectly sharp, but has a small radius at the tool tip. These are both factors that could be considered in future studies.

In addition, it would worthwhile to investigate the capabilities of other software packages. The software package used in this work, DYNA3D, was still in the developmental stage when it was distributed. An updated version of DYNA3D, LS-DYNA, is now commercially available and may be better suited for this project. LS-DYNA is faster and more reliable than DYNA3D and has expanded capabilities.

Unfortunately, it would not be possible to modify the source code if LS-DYNA was used. As a result, there would be no way to add the distance criterion to the element separation criteria. The element separation criterion would then be based entirely on the shear and normal stresses in the element. However, it may be possible to run the simulations effectively without the distance criterion. Since the separation criterion is somewhat arbitrary and does not exactly represent real life, it may be possible to obtain similar results without the distance criterion by adjusting the shear and normal failure stresses for the elements. Some trial and error would be necessary to determine appropriate values.

While the majority of machining models have focused on orthogonal cutting, the majority of machining operations performed in industry are oblique cutting operations. Preliminary work has been done in developing an oblique cutting simulation. Figures 4.1 and 4.2 depict an oblique cutting simulation developed by the author using the power law strain hardening material model. This simulation is in the early stages of development and would provide another fertile area for researchers to investigate in the future.

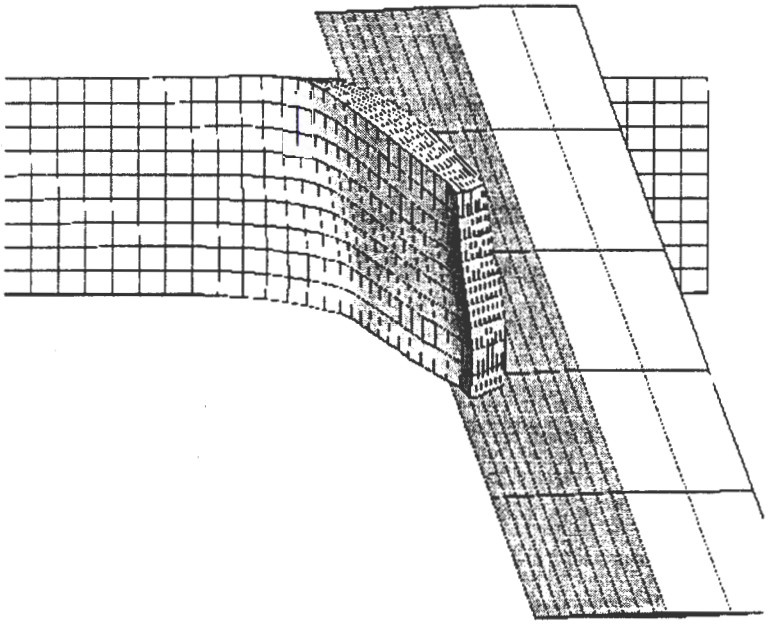

Figure 4.1 Top view of oblique cutting simulation

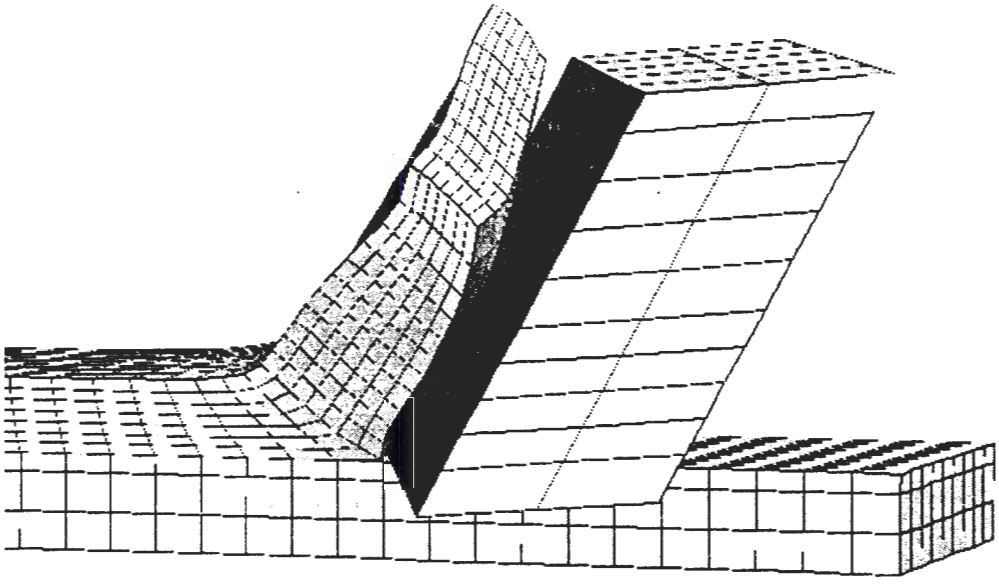

Figure 4.2 Side view of oblique cutting simulation

4.3 Conclusion

This thesis has detailed the early development of a finite element metal cutting simulation. Although the metal cutting process is quite complex and further work is needed to create an entirely accurate machining model, the simulations in this paper have provided useful results. Simulations have been developed which accurately depict chip curl in orthogonal machining and show the effects of groove geometry on chip formation. In addition, improvements to the model have been made which account for the effects of strain rate hardening and thermal softening. These simulations have been shown to accurately predict experimentally measured cutting forces and hold much potential for the future.

APPENDIX A CREATING MACHINING SIMULATIONS WITH DYNA3D

The contents of this appendix explain in detail the method used to create models and run simulations using DYNA3D. The basic steps involved in the process are illustrated in Fig. A.1. Three programs are needed to generate the simulations and view the results. The preprocessor, called Ingrid, creates a finite element mesh and generates an input file to be used by DYNA3D. DYNA3D does the actual number crunching, calculating the final deformed shape of the workpiece and any other desired information. Finally, the results are viewed with the postprocessor, called Griz. Executable files for these programs are all available on the ICEMT (Iowa Center for Emerging Manufacturing Technology) SGI system in the directory /home/software/llnl_codes. Additional instructions for installing the software may be found in the file /home/software/llnl_codes/source/Sgi/Installation.ps.

The first step in the simulation process is to create an input file for the Ingrid preprocessor. This file is a text file defining the geometry of the problem, along with any boundary conditions. Sample Ingrid input files for several simulations are found in Appendices B-E. Once the input file is generated, Ingrid is started by issuing the following command at the Unix prompt:

ingrid i=file

where file is the name of the input file. Many commands are available in Ingrid for viewing the mesh and the workpiece. The only command that must be used in Ingrid is the command to generate the DYNA3D output file. This is done by typing 'continue' at the Ingrid prompt. Ingrid will then generate a file called 'ingrido' which can be read by DYNA3D.

Once the output file is generated, the simulation may be run on DYNA3D by typing the following command at the Unix prompt:

dyna3d i=ingrido

DYNA3D will perform all the calculations for the simulation and generate several output files. Binary data files, called d3plot, will be written. It is also possible to output other files including data such as the nodal forces acting on specified surfaces. When DYNA3D has finished running, it will generate a restart file called d3dump01. If it is desired to continue the simulation, DYNA3D may be

restarted by issuing the following command at the Unix prompt:

dyna3d r=d3dump01

Once DYNA3D has generated the binary data files, the results may be viewed using the postprocessor Griz. Griz creates a visual display of the simulation results. It is possible to view the deformed geometry along with contours of important data, such as stresses and strains. Griz is opened by issuing the following command at the Unix prompt:

griz -i d3plot

Modification of the DYNA3D Source Code

For this research project, the DYNA3D source code was modified in order to add a geometric criterion to the element separation algorithm. This was accomplished by modifying the subroutine slavf2.f. Appendix F contains the modified version of the subroutine used for the orthogonal cutting simulations performed for this work. Appendix G contains a modified version of the subroutine developed for a possible extension of the simulation to include oblique metal cutting. Appendix H contains step by step instructions for compiling a modified version of DYNA3D for use on the SGI workstations, and Appendix I contains the instructions for compiling a version to run on a DEC station. Although DYNA3D may be run on a DEC station, it is still necessary to use the SGI workstations to run the programs Ingrid and Griz. It is important to note that the binary mode should be used to transfer the DYNA3D data files via ftp from a DEC station to an SGI workstation. If the ascii mode is used, Griz will not be able to read the data files.

Correcting the DYNA3D Input File

The Ingrid input file for the simulations using Johnson-Cook material properties will not generate all the information needed to run the simulation with DYNA3D. As a result, it is necessary to manually make some modifications to the DYNA3D input file, called ingrido. The modified portion of the file is shown in Appendix J. The first value that must be modified is the value of the material constant C. One other flag in the ingrido file must be modified if it is desired to output the forces on the surface of the tool.

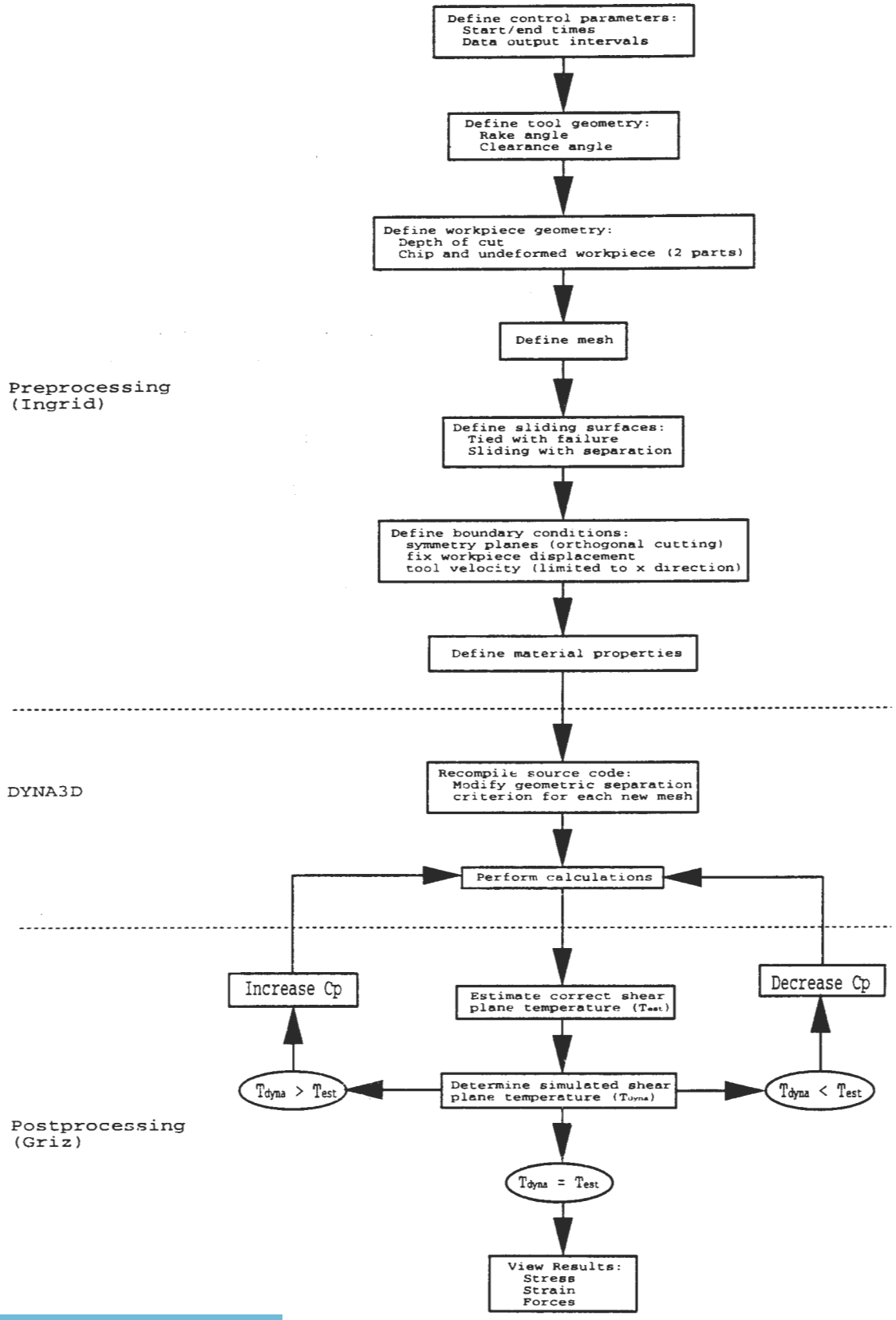

Figure A.1 Method for creating simulations

APPENDIX B INGRID INPUT FILE FOR FLAT FACED TOOL SIMULATION

Note: This is the input file for the flat faced tool simulation in the first paper.

```
c Simulation title.  All units are given in terms of grams, cm, and microseconds
Metal cutting simulation (gm cm microsec)
c Input file will be generated for DYNA3D
dn3d
c Simulation ends at 60,000 microseconds
term 60000
c Data will be stored at intervals of 40 microseconds in the simulation
plti 40
prti 40
c Define 3 slide surfaces: #1 - sliding with separation and friction
c   slide surface with coefficient of friction = 0.1, #2 - tied with failure
c   slide surface to model separation of chip from workpiece, #3 - dummy
c   slide surface for the bottom of the tool
si 1 sv fric 0.1;
si 2 break;
si 3 dummy;
c Define load curve #1 with a value of 1 at time 0 and at time 60001
c   (constant load).  Will be used to define tool velocity
lcd  1 2 0 1 60001 1
c Define symmetry planes to constrain deformation to the x and y directions
plane 2  0 0 0 0 0 1 0.001 symm
         0 0 -0.008467 0 0 -1 0.001 symm


c Start defining the first of three parts (the tool)
start
c Define part as block with 3 nodes in x, 11 nodes in y, and 2 nodes in
c   z directions
1 3; 1 11; 1 2;
c Coordinates for nodes 1 and 3 in x direction, nodes 1 and 11 in y
c   direction, and nodes 1 and 2 in z direction
0.0 0.025  0.0 0.08  0.005 -0.013467
c Rotate front face of tool -30 degrees around z-axis
rr 1 1 1 1 2 2  rz  -30;
c Translate back of tool -0.0025cm in x direction, rotate it 30 degrees,
c   and translate it back
rr 2 1 1 2 2 2  mx -0.025  rz -30  mx 0.025;
c Rotate bottom of tool 5 degrees about z-axis
rr 1 1 1 2 1 2  rz 5;
c Translate top of toop -0.08cm in y direction, rotate 5 degrees, and
```

```
c   translate back
rr 1 2 1 2 2 2  my -0.08 rz 5 my 0.08;
c Limit movement of the tool to the x direction
b 1 1 1 2 2 2  011111
c Translate tool 0.001cm in the x direction
mb 0 0 0 0 0 0  x 0.001
c Define front of tool as master surface for sliding interface #1
si 1 1 1 1 2 2  1 m
c Define bottom of tool as master surface for sliding interface #2
sii 1 2 ; 1 1 ; 1 2 ;  3  m
c Define tool velocity.  Velocity in x direction equal to -2.63e-5 times
c   load curve #1 (constant velocity of -2.63e-5).  Velocity in y and z
c   directions equal to zero.
fv 1 1 1 2 2 2  1  -2.63e-5 1 0 0
c Tool is made out of material #1
mate 1
c End of tool definition
end


c Define second part (portion of workpiece which forms the chip)
start
c Define as block with 51 nodes in x direction, 8 nodes in y direction,
c   and 2 nodes in z direction
1 50 51; 1 8; 1 2;
c Coordinates for nodes 1, 50, and 51 in x direction, 1 and 8 in 8
c   direction, and 1 and 2 in z direction
-0.1568 -0.0032 0  0 0.025  0 -0.008467
c Fix the left end of the part (no translation or rotation)
b 1 1 1 1 2 2  111111
c Translate top of the part -0.004cm in x direction (tilts the elements)
mb 1 2 1 3 2 2  x  -0.004
c Define as slave surface of sliding interface #1
sii 1 -3; -1 2; 1 2; 1 s
c Define bottom of chip as slave surface of sliding interface #2.  The
c   terms 0.00345 and 0.00199 give the shear and normal failure forces for
c   use with the element separation criterion
sii 1 3; 1 1; 1 2; 2 s 0.00345 0.00199
c Chip is made out of material #2
mate 2
c End of second part definition
end


c Define third part (forms finished surface of the workpiece)
start
c Define block of nodes as before
1 50 51; 1 3 4 ; 1 2;
-0.1568 -0.0032 0.0  -0.0254 -0.005 0  0 -0.008467
c Apply boundary conditions fixing the workpiece location
b 1 1 1 1 3 2  111111
b 1 1 1 3 1 2  111111
b 1 1 1 3 3 2  011111
```

```
c Define top of part as master surface of sliding interface #2
sii 1 3; 3 3; 1 2; 2 m
c Define top of part as slave surface of sliding interface #3
sii 1 3; 3 3; 1 2; 3 s
c Part is made out of material #2
mate 2
c End of part definition
end


c Define material #1 to be a Type 1 material.  (Type 1 is an Elastic material.)
mat 1 1
c Define material properties: Young's modulus (e), density (ro),
c   Poisson's ratio (pr).  Note: Young's modulus was defined as an
c   arbitrarily high number in order to make the tool rigid.
ro 7.801
e 8
pr 0.3
c End of material #1 definition
endmat


c Define material #2 to be a Type 18 material.  (Type 18 is a power law
c  strain hardening model.)
mat 2 18
c Define material properties: Young's modulus (e), density (ro),
c   Poisson's ratio (pr), strength coefficient (k), and strain hardening
c   exponent (n).
e 2.069
ro 7.801
pr 0.29
k 0.0082
n 0.285
c End of material #2 definition
endmat
c End of Ingrid input file
end
```

APPENDIX C INGRID INPUT FILE FOR GROOVED TOOL SIMULATION

Note: this is the input file for Simulation 2b in the first paper

```
Metal cutting simulation (gm cm microsec)
dn3d
term 60000
plti 40
prti 40
si 1 sv fric 0.1;
si 2 break;
si 3 dummy;
si 4 sv;
lcd  1 2 0 1 60001 1
plane 2  0 0 0 0 0 1 0.001 symm
         0 0 -0.008467 0 0 -1 0.001 symm


start
1 2 3; 1 2 6 10 11; 1 2;
0.0 0.025 0.04  0.0 0.0125 0.05 0.1 0.11  0.005 -0.013467
rr 1 1 1 3 1 2  rz 5;
rr 1 2 1 3 2 2  my -0.0125 rz 5 my 0.0125;
rr 1 3 1 3 3 2  my -0.05 rz 5 my 0.05;
rr 1 4 1 3 4 2  my -0.1 rz 5 my 0.1;
rr 1 5 1 3 5 2  my -0.11 rz 5 my 0.11;
sfi 1 ; 1 4 ; ; cy -0.069125 0.05 0  0 0 1  0.086125
b 1 1 1 3 5 2  011111
mb 0 0 0 0 0 0  x 0.001
si 1 1 1 1 5 2  1 m
sii 1 3 ; 1 1 ; 1 2 ;  3  m
fv 1 1 1 1 5 2  1  -2.63e-5 1 0 0
mate 1
end

start
1 75 76; 1 7; 1 2;
-0.381 -0.00508 0   0 0.025   0 -0.008467
b 1 1 1 1 2 2  111111
mb 1 2 1 3 2 2  x -0.004
sii 1 -3; -1 2; 1 2;  1 s
sii 1 2; 1 1; 1 2; 2 s 0.00345 0.00199
mate 2
end
```

```
start
1 75 76; 1 3 4 ; 1 2;
-0.381 -0.00508 0  -0.0254 -0.00508 0   0 -0.008467
b 1 1 1 1 3 2  111111
b 1 1 1 3 1 2  111111
b 1 1 1 3 3 2  011111
sii 1 2; 3 3; 1 2; 2 m
sii 1 3; 3 3; 1 2; 3 s
mate 2
end


mat 2 18
e 2.069
ro 7.801
pr 0.29
k 0.0082
n 0.285
endmat


mat 1 1
ro 7.801
e 8
pr 0.3
endmat
end
```

APPENDIX D INGRID INPUT FILE FOR SIMULATION WITH JOHNSON-COOK CONSTITUTIVE MODEL

Note: This is the input file for Case 4 in the second paper.

```
Metal cutting simulation (gm cm microsec)
dn3d
term 60000
plti 3
prti 3
si 1 sv fric 0.1;
si 2 break;
si 3 dummy;
si 4 sv fric 0.3;
lcd  1 2 0 1 60001 1
plane 2  0 0 0 0 0 1 0.001 symm
         0 0 -0.008467 0 0 -1 0.001 symm


start
1 3; 1 12; 1 2;
0.0 0.025  0.0 0.1  0.005 -0.013467
rr 1 1 1 2 1 2  rz 5;
b 1 1 1 2 2 2  011111
mb 0 0 0 0 0 0  x 0.001
si 1 1 1 1 2 2  1 m
sii 1 2 ; 1 1 ; 1 2 ;  3  m
fv 1 1 1 2 2 2  1  -4.064e-4 1 0 0
mate 1
end


start
1 80 81; 1 10; 1 2;
-0.256 -0.0032 0  0 0.01524  0 -0.008467
b 1 1 1 1 2 2  111111
mb 1 2 1 3 2 2  x  -0.002
sii 1 -3; -1 2; 1 2; 1 s
sii 1 3; 1 1; 1 2; 2 s 0.00345 0.00199
mate 2
end


start
1 80 81; 1 3 4 ; 1 2;
```

```
-0.256 -0.0032 0.0  -0.0254 -0.005 0  0 -0.008467
b 1 1 1 1 3 2  111111
b 1 1 1 3 1 2  111111
b 1 1 1 3 3 2  011111
sii 1 3; 3 3; 1 2; 2 m
sii 1 3; 3 3; 1 2; 3 s
mate 2
end


mat 2 15
ro 7.801
g 0.83
a 0.003913
b 0.007239
n 0.3067
C 0.1144
m 0.9276
tm 1728
tr 294
x0 0.0000653
sh 0.00000477
pmin -1000
d1 100
d2 0
d3 0
d4 0
d5 0
endmat


eos 2 1
c0 0
c1 2
c2 0
c3 0
c4 0
c5 0
c6 0
e0 0
v0 1
endeos


mat 1 1
ro 7.801
e 8
pr 0.3
endmat
end
```

APPENDIX E INGRID INPUT FILE FOR OBLIQUE CUTTING SIMULATION

Note: This is the input file for the oblique cutting simulation in Chapter 4.

```
Metal cutting simulation (gm cm microsec)
dn3d
term 40000
plti 40
prti 40
si 1 sv fric 0.1;
si 2 break;
si 3 dummy;
si 4 sv;
lcd  1 2 0 1 60001 1


start
1 2 3; 1 2 6 10 11; 1 6;
0.0 0.03 0.06  0.0 0.0125 0.05 0.1 0.11  0.2 -0.08
rr 1 1 1 1 5 2 rz -30;
rr 2 1 1 2 5 2 mx -0.03 rz -30 mx 0.03;
rr 3 1 1 3 5 2 mx -0.06 rz -30 mx 0.06;
rr 1 1 1 3 1 2  rz 5;
rr 1 2 1 3 2 2  my -0.0125 rz 5 my 0.0125;
rr 1 3 1 3 3 2  my -0.05 rz 5 my 0.05;
rr 1 4 1 3 4 2  my -0.1 rz 5 my 0.1;
rr 1 5 1 3 5 2  my -0.11 rz 5 my 0.11;
b 1 1 1 3 5 2  011111
mb 0 0 0 0 0 0  x 0.001
mb 1 1 1 1 5 1  x 0.101912
mb 2 1 1 2 5 1  x 0.101912
mb 3 1 1 3 5 1  x 0.101912
si 1 1 1 1 5 2  1 m
sii 1 3 ; 1 1 ; 1 2 ;  3  m
fv 1 1 1 1 5 2  1  -2.63e-5 1 0 0
mate 1
end


start
1 40 41; 1 8; 1 10;
-0.5 -0.0125 0   0 0.02   0.05 -0.05
b 1 1 1 1 2 2  111111
mb 1 2 1 3 2 2  x -0.002
```

```
mb 1 2 1 3 2 2  x -0.000448
sii 1 -3; -1 2; 1 2;  1 s
sii 1 2; 1 1; 1 2; 2 s 0.00345 0.00199
mate 2
end


start
1 40 41; 1 3 4; 1 10;
-0.5 -0.0125 0  -0.0254 -0.00508 0    0.05 -0.05
b 1 1 1 1 3 2  111111
b 1 1 1 3 1 2  111111
b 1 1 1 3 3 2  111111
sii 1 2; 3 3; 1 2; 2 m
sii 1 3; 3 3; 1 2; 3 s
mate 2
end

ihq 5


mat 2 18
e 2.069
ro 7.801
pr 0.29
k 0.0082
n 0.285
endmat


mat 1 1
ro 7.801
e 8
pr 0.3
endmat
end
```

APPENDIX F MODIFIED DYNA3D SUBROUTINE SLAVF2.F FOR ORTHOGONAL CUTTING SIMULATION

```
************************************************************************
*    Modified from original to incorporate geometrical (distance)     *
*    and physical (eq. 270, pg. 269 DYNA3D manual) criteria for metal *
*    cutting. Physical criteria is in the original version. Few lines *
*    were added to incorporate the geometrical criteria.              *
************************************************************************


      subroutine slavf2(x,e,irect,lmsr,msr,nsv,iloc,irtl,stf,
     1 nsn,nmn,nty,fdat,iseg,fric,nseg,failz,crst)
#ifdef DP
      implicit double precision (a-h,o-z)                                dp
#endif
      common/sl19/llc,lrsort,resltl,result,i,k,m,n
      common/bk02/dt1,dt2,iburn,isdo,iorder
      common/bk09/det,h(20),p1(20),p2(20),p3(20),aj(9),eps(9)
      common/bk11/ux(20),uy(20),uz(20),xx1(20),xx2(20),xx3(20)
      common/bk14/xs1,ys1,zs1,sig(3),epx,mx,ix(10),iy(10)
      common/bk21/amx,amy,amz,fs1,fs2,fs3,ft1,ft2,ft3,sp,sm,tp,tm
      logical first_cyc
      common/bk26/first_cyc
      common/bk28/summss,xke,xpe,timx
      common/slv2/thk,isrch
      common/double/iprec,ncpw,unit
      dimension x(3,*),e(*),irect(4,*),lmsr(*),msr(*),nsv(*),iloc(*),
     1 irtl(*),stf(*),fdat(5,*),iseg(*),fric(*),failz(5,*),crst(2,*)
      data zero /0.0/
      fcoeff=fric(1)**2+fric(2)**2+fric(3)**2

************************************************************************
*                                                                      *
*  New Lines added to code.  Note: Set variable distcri equal to 10% *
*  times the element length.  Variable xtool gives tool position.     *
*                                                                      *
      xtool = x(1,1)
      distcri = 0.00016
*                                                                      *
************************************************************************


      do 100 ii=1,nsn
      i=nsv(ii)
```

```
      j=iloc(ii)
      k=msr(j)
      l=irtl(ii)
      do 10 jj=1,4
      nn=irect(jj,l)
      ix(jj)=nn
      xx1(jj)=x(1,nn)
      xx2(jj)=x(2,nn)
   10 xx3(jj)=x(3,nn)
      xs1=x(1,i)
      ys1=x(2,i)
      zs1=x(3,i)
      if (failz(1,ii).eq.0) then
      if (k.ne.ix(1)) go to 20
      k1=1
      k2=2
      k3=4
      go to 50
   20 if (k.ne.ix(2)) go to 30
      k1=2
      k2=3
      k3=1
      go to 50
   30 if (k.ne.ix(3)) go to 40
      k1=3
      k2=4
      k3=2
      if (ix(3).eq.ix(4)) k2=1
      go to 50
   40 if (k.ne.ix(4)) go to 50
      k1=4
      k2=1
      k3=3
   50 call ptime (k1,k2,k3,detv)
      if (detv.gt.0.) go to 80
      endif
      ierr=0
      i3=3*i
      i2=i3-1
      i1=i2-1
      call stex (xn1;xn2,xn3,ss,tt,ierr,0)
      ans=xn1*(xs1-amx)+xn2*(ys1-amy)+xn3*(zs1-amz)
      if (failz(1,ii).gt.0.0) then
      if (first_cyc) then
       if (ierr.ne.0) then
        failz(1,ii)=0.0
        go to 80
       endif
      crst(1,ii)=ss
      crst(2,ii)=tt
      x(1,i)=amx
      x(2,i)=amy
      x(3,i)=amz
```

```
      ans=0.0
      failz(5,ii)=float(l)
      else
      jj=nint(failz(5,ii))
      tp=.25*(1.0+crst(2,ii))
      tm=.25*(1.0-crst(2,ii))
      sp=1.0+crst(1,ii)
      sm=1.0-crst(1,ii)
      h1=tm*sm
      h2=tm*sp
      h3=tp*sp
      h4=tp*sm
      nn1=irect(1,jj)
      nn2=irect(2,jj)
      nn3=irect(3,jj)
      nn4=irect(4,jj)
      dx=x(1,i)-h1*x(1,nn1)-h2*x(1,nn2)-h3*x(1,nn3)-h4*x(1,nn4)
      dy=x(2,i)-h1*x(2,nn1)-h2*x(2,nn2)-h3*x(2,nn3)-h4*x(2,nn4)
      dz=x(3,i)-h1*x(3,nn1)-h2*x(3,nn2)-h3*x(3,nn3)-h4*x(3,nn4)
      fxi=stf(l)*dx
      fyi=stf(l)*dy
      fzi=stf(l)*dz
      frcmag=fxi*fxi+fyi*fyi+fzi*fzi
      frcnrm=fxi*xn1+fyi*xn2+fzi*xn3
      frctan=sqrt(max(frcmag-frcnrm**2,zero))
      fltest=(  max(zero,frcnrm)/failz(1,ii))**failz(3,ii)
     1      +(         frctan /failz(2,ii))**failz(4,ii)

*********************************************************************
*                                                                   *
* New lines added to code, adding distance to the failure criteria *
*                                                                   *
     dist = abs( xs1 - xtool )

      if ((dist.le.distcri.and.fltest.gt.1.0).or.dist.le.0) then
fltest = 1.5
      else
fltest = 0.5
      endif
*                                                                   *
*********************************************************************

      if (fltest.gt.1.0) then
      write (13,120) ii,i,timx,frcnrm,frctan
      failz(1,ii)=0.
      failz(2,ii)=0.
      go to 58
      endif
      endif
      go to 68
      endif
   58 if (ierr.eq.0.and.ans.gt.0.) go to 80
      if (isrch.eq.1) call thkgs(xx1,xx2,xx3,thk)
```

```
      if ((ierr.ne.0.and.  max(abs(ss),abs(tt)).le.2.).or.
     1    ans.lt.-thk)
     1 call salvex(ans,i,ierr,xn1,xn2,xn3,ss,tt,l,x,irect,lmsr,
     1             msr,nseg,nmn)
      if (ierr.ne.0.or.ans.gt.0..or.ans.lt.-thk) go to 80
   60 fni=ans*stf(l)
      fxi=xn1*fni
      fyi=xn2*fni
      fzi=xn3*fni
      if (fcoeff.eq.0.0) go to 68
      jj=iseg(ii)
      if (jj.ne.0) go to 65
      iseg(ii)=l
      fdat(1,ii)=ss
      fdat(2,ii)=tt
      go to 68
   65 tp=.25*(1.0+fdat(2,ii))
      tm=.25*(1.0-fdat(2,ii))
      sp=1.0+fdat(1,ii)
      sm=1.0-fdat(1,ii)
      h1=tm*sm
      h2=tm*sp
      h3=tp*sp
      h4=tp*sm
      nn1=irect(1,jj)
      nn2=irect(2,jj)
      nn3=irect(3,jj)
      nn4=irect(4,jj)
      dx=amx-h1*x(1,nn1)-h2*x(1,nn2)-h3*x(1,nn3)-h4*x(1,nn4)
      dy=amy-h1*x(2,nn1)-h2*x(2,nn2)-h3*x(2,nn3)-h4*x(2,nn4)
      dz=amz-h1*x(3,nn1)-h2*x(3,nn2)-h3*x(3,nn3)-h4*x(3,nn4)
      vel=sqrt(dx**2+dy**2+dz**2)/  max(1.e-20*unit,dt2)
      fdat(3,ii)=fdat(3,ii)+stf(l)*dx
      fdat(4,ii)=fdat(4,ii)+stf(l)*dy
      fdat(5,ii)=fdat(5,ii)+stf(l)*dz
      proj=fdat(3,ii)*xn1+fdat(4,ii)*xn2+fdat(5,ii)*xn3
      fdat(3,ii)=fdat(3,ii)-proj*xn1
      fdat(4,ii)=fdat(4,ii)-proj*xn2
      fdat(5,ii)=fdat(5,ii)-proj*xn3
      fmax=-(fric(2)+(fric(1)-fric(2))*exp(-fric(3)*vel))*fni
      fmag=sqrt(fdat(3,ii)**2+fdat(4,ii)**2+fdat(5,ii)**2)
      if (fmax.ge.fmag.or.fmag.eq.0.) go to 67
      sclf=fmax/fmag
      fdat(3,ii)=sclf*fdat(3,ii)
      fdat(4,ii)=sclf*fdat(4,ii)
      fdat(5,ii)=sclf*fdat(5,ii)
   67 fxi=fxi+fdat(3,ii)
      fyi=fyi+fdat(4,ii)
      fzi=fzi+fdat(5,ii)
      iseg(ii)=l
      fdat(1,ii)=ss
      fdat(2,ii)=tt
   68 do 70 jj=1,4
```

```
      j3=3*ix(jj)
      j2=j3-1
      j1=j2-1
      e(j1)=e(j1)+fxi*h(jj)
      e(j2)=e(j2)+fyi*h(jj)
      e(j3)=e(j3)+fzi*h(jj)
   70 continue
      e(i1)=e(i1)-fxi
      e(i2)=e(i2)-fyi
      e(i3)=e(i3)-fzi
      go to 100
   80 if (fcoeff.eq.0.0) go to 100
      iseg(ii)=0
      fdat(3,ii)=0.
      fdat(4,ii)=0.
      fdat(5,ii)=0.
  100 continue
      return
  120 format(//,' slave node number ',i8,' node number ',
     1  i8,' has failed',/,' at time: ',1pe12.4,/,
     2 ' the normal force was: ', 1pe12.4,/,
     3 ' the tangential force was: ', 1pe12.4,///)
      end
```

APPENDIX G MODIFIED SUBROUTINE SLAVF2.F FOR OBLIQUE CUTTING SIMULATION

```
************************************************************************
*    Modified from original to incorporate geometrical (distance)      *
*    and physical (eq. 270, pg. 269 DYNA3D manual) criteria for oblique *
*    metal cutting. Most of subroutine is the same as the orthogonal    *
*    version, so some unmodified sections have been left out for brevity *
************************************************************************


      subroutine slavf2(x,e,irect,lmsr,msr,nsv,iloc,irtl,stf,
     1 nsn,nmn,nty,fdat,iseg,fric,nseg,failz,crst)
#ifdef DP
      implicit double precision (a-h,o-z)                                dp
#endif
      common/sl19/llc,lrsort,resltl,result,i,k,m,n
      common/bk02/dt1,dt2,iburn,isdo,iorder
      common/bk09/det,h(20),p1(20),p2(20),p3(20),aj(9),eps(9)
      common/bk11/ux(20),uy(20),uz(20),xx1(20),xx2(20),xx3(20)
      common/bk14/xs1,ys1,zs1,sig(3),epx,mx,ix(10),iy(10)
      common/bk21/amx,amy,amz,fs1,fs2,fs3,ft1,ft2,ft3,sp,sm,tp,tm
      logical first_cyc
      common/bk26/first_cyc
      common/bk28/summss,xke,xpe,timx
      common/slv2/thk,isrch
      common/double/iprec,ncpw,unit
      dimension x(3,*),e(*),irect(4,*),lmsr(*),msr(*),nsv(*),iloc(*),
     1 irtl(*),stf(*),fdat(5,*),iseg(*),fric(*),failz(5,*),crst(2,*)
      data zero /0.0/
      fcoeff=fric(1)**2+fric(2)**2+fric(3)**2

************************************************************************
*                                                                      *
*  New lines added to code.  Variable x(*,*) represents nodal position*
*  of leading edge of tool.  Variable dvector* will be used to calcu- *
*  late distance between nodal coordinates on workpiece and the line  *
*  representing the leading edge of the tool.  Variable distcri should*
*  be set equal to 10% times the element length.       *
*                                                                      *
      nsecond = 2
      dvectorx = x(1,1) - x(1,nsecond)
      dvectory = x(2,1) - x(2,nsecond)
      dvectorz = x(3,1) - x(3,nsecond)
```

```
*       distcri = 0.00024 =  10% of length of 0.0024 long elements
distcri = 0.00024
*                                                                     *
**********************************************************************

      do 100 ii=1,nsn
      i=nsv(ii)
      j=iloc(ii)
      k=msr(j)
                        .

                        .

                        .

      frcnrm=fxi*xn1+fyi*xn2+fzi*xn3
      frctan=sqrt(max(frcmag-frcnrm**2,zero))
      fltest=(  max(zero,frcnrm)/failz(1,ii))**failz(3,ii)
     1      +(         frctan /failz(2,ii))**failz(4,ii)

**********************************************************************
*                                                                     *
*  New lines added to code.  Vector operations are used to calculate  *
*  the distance from nodal points on workpiece to line representing   *
*  the position of the leading edge of the tool, represented by the   *
*  variable ''dist''.                                                 *
*                                                                     *
      vecmatx = xs1 - x(1,1)
      vecmaty = ys1 - x(2,1)
      vecmatz = zs1 - x(3,1)
      upperi = vecmaty*dvectorz - vecmatz*dvectory
      upperj = vecmatz*dvectorx - vecmatx*dvectorz
      upperk = vecmatx*dvectory - vecmaty*dvectorx

      dnumedist = (upperi*upperi + upperj*upperj +
     1             upperk*upperk)**(0.5)
      ddenodist = (dvectorx*dvectorx + dvectory*dvectory +
     1            dvectorz*dvectorz)**(0.5)
      dist = dnumedist/ddenodist
*                                                                     *
**********************************************************************

**********************************************************************
*                                                                     *
*  Line modified from original to include geometric separation criteria*
*                                                                     *
      if ((dist.le.distcri.and.fltest.gt.1.0).or.dist.le.0) then
*                                                                     *
**********************************************************************

      write (13,120) ii,i,timx,frcnrm,frctan
      failz(1,ii)=0.
      failz(2,ii)=0.
```

```
      .
      .
      .
120 format(//,' slave node number ',i8,' node number ',
   1  i8,' has failed',/,' at time: ',1pe12.4,/,
   2 ' the normal force was: ', 1pe12.4,/,
   3 ' the tangential force was: ', 1pe12.4,///)
    end
```

APPENDIX H COMPILING MODIFIED DYNA3D CODES ON SGI WORKSTATIONS

```
1) Create directory called LLNL_CODES
2) In the LLNL_CODES directory:

   Create directory call Diglib

3) In the Diglib direcory:
   copy files (from ICEMT SGI account):
     /home/software/llnl_codes/source/Sgi/devindep_f.sgi
     /home/software/llnl_codes/source/Sgi/x11_f.sgi
     /home/software/llnl_codes/source/Sgi/x11_c.sgi

   Enter the following commands:
     fsplit devindep_f.sgi
     fsplit x11_f.sgi
     f77 -c -old_rl -static -O2 -G 0 *.f
     cc -c -O2 x11.c
     ar r libdiglib_sgi.a *.o


4) In the LLNL_CODES directory:

   Create directory call Dyna3d

5) In the Dyna3d direcory:
   copy files (from ICEMT SGI account):

     /home/software/llnl_codes/source/Common/dyna3d.F
     /home/software/llnl_codes/source/Common/dyna3d.mk
     /home/software/llnl_codes/source/Common/llnlcode.mk


   Note: The following lines in dyna3d.mk must be modified.

       Comment out lines 276 and 277:
       276 fsplit$(SOBJS)
       277 -rm zzz*.f

       Modify line 313:
       Original
       ls *.f|awk 'BEGIN{printf''DOBJS =''}{printf''
       \\\n\t''$(SGILS)1}END{printf''\n''}'>&! Listfile.mk
```

```
    Modified:
    ls *.f|awk 'BEGIN{printf''DOBJS =''}{printf''
    \\\n\t''$$1}END{printf''\n''}'>&! Listfile.mk

After modifying dyna3d.mk, enter command:  fsplit dyna3d.F
Replace subroutine slavf2.f with modified version
Enter command:  make -f dyna3d.mk SGI
Change executable file ddyna3d.sgi to desired name
```

APPENDIX I COMPILING MODIFIED DYNA3D CODES ON DEC WORKSTATIONS

```
1) Create directory called LLNL_CODES
2) In the LLNL_CODES directory:

   Create directory call Diglib

3) In the Diglib direcory:
   copy files (from ICEMT SGI account):
     /home/software/llnl_codes/source/Sgi/devindep_f.sgi
     /home/software/llnl_codes/source/Sgi/x11_f.sgi
     /home/software/llnl_codes/source/Sgi/x11_c.sgi

   Enter the following commands:
     fsplit devindep_f.sgi
     fsplit x11_f.sgi
     f77 -c -assume byterecl -convert big_endian -static -O2 -G 0 *.f
     cc -c -O2 x11.c
     ar r libdiglib_sgi.a *.o

4) In the LLNL_CODES directory:

   Create directory called Dyna3d

5) In the Dyna3d direcory:
   copy files (from ICEMT SGI account):

     /home/software/llnl_codes/source/Common/dyna3d.F
     /home/software/llnl_codes/source/Common/dyna3d.mk
     /home/software/llnl_codes/source/Common/llnlcode.mk


   Note: The following lines in dyna3d.mk must be modified.
       Modify line 175:
       Original
       DECFCFL  = -c -O -G 0 -cpp $(DEBUG)
       Modified
       DECFCFL  = -c -assume byterecl -convert big_endian -O -G 0 -cpp $(DEBUG)

       Comment out lines 294 and 295:
       276 fsplit$(SOBJS)
       277 -rm zzz*.f

       Modify line 324:
```

```
Original
a2.dec:
ls *.f|awk 'BEGIN{printf''DOBJS =''}{printf''
\\\n\t''$(DECLS)1}END{printf''\n''}'> Listfile.mk

Modified:
ls *.f|awk 'BEGIN{printf''DOBJS =''}{printf''
\\\n\t''$$1}END{printf''\n''}'>&! Listfile.mk
```

```
After modifying dyna3d.mk, enter command:  fsplit dyna3d.F
Replace subroutine slavf2.f with modified version
Enter command:  make -f dyna3d.mk DEC
Change executable file ddyna3d.dec to desired name
```

APPENDIX J MODIFICATIONS MADE TO DYNA3D INPUT FILE "INGRIDO"

Addition of missing material propterties

Due to a glitch in the program, the Ingrid preprocessor does not read in the value for the Johnson/Cook material constant "C". It interprets this command as a comment. As a result, it is necessary to manually enter the value for C in the "ingrido" input file under the material cards section. For O1 tool steel, the value of C is 0.1144, and it may be entered by modifying one entry as follows.

Unmodified input file:

```
*
*-------------------------- MATERIAL CARDS --------------------------*
*

                                    .
                                    .
                                    .

material type # 15 (Johnson/Cook Strain and Tempurature Sensitive Plasticity)
8.300E-01 3.913E-03 7.239E-03 3.067E-01 0.000E+00 9.276E-01 1.728E+03 2.940E+02
```

Modified line:

```
material type # 15 (Johnson/Cook Strain and Tempurature Sensitive Plasticity)
8.300E-01 3.913E-03 7.239E-03 3.067E-01 1.144E-01 9.276E-01 1.728E+03 2.940E+02
```

Writing forces on rake face to a file

In order to output the forces on the rake face of the tool, it is necessary to modify one control card in the "ingrido" input file. Changing the zero to a one instructs DYNA3D to write a data file called "forces" which will contain the forces acting on the master surface of this sliding interface. In this case, the master surface is the rake face of the tool.

Unmodified portion of input file:

```
*
*---------------------- SLIDING INTERFACE DEFINITIONS ----------------------*
*
     89       11     3 1.000E-01 0.000E+00 0.000E+00     0     0    00.0E+000.0E+00
```

Modified line:

```
*
*---------------------- SLIDING INTERFACE DEFINITIONS ----------------------*
*
     89       11     3 1.000E-01 0.000E+00 0.000E+00     0     0    10.0E+000.0E+00
```